

Persistent-Homology-based Machine Learning and its Applications – A Survey

Chi Seng Pun*

*School of Physical and Mathematical Sciences
Nanyang Technological Technology
Singapore 637371*

CSPUN@NTU.EDU.SG

Kelin Xia*

*School of Physical and Mathematical Sciences
and School of Biological Sciences
Nanyang Technological Technology
Singapore 637371*

XIAKELIN@NTU.EDU.SG

Si Xian Lee

*School of Physical and Mathematical Sciences
Nanyang Technological Technology
Singapore 637371*

LEES0159@E.NTU.EDU.SG

Editor: TBC

Abstract

A suitable feature representation that can both preserve the data intrinsic information and reduce data complexity and dimensionality is key to the performance of machine learning models. Deeply rooted in algebraic topology, persistent homology (PH) provides a delicate balance between data simplification and intrinsic structure characterization, and has been applied to various areas successfully. However, the combination of PH and machine learning has been hindered greatly by three challenges, namely topological representation of data, PH-based distance measurements or metrics, and PH-based feature representation. With the development of topological data analysis, progresses have been made on all these three problems, but widely scattered in different literatures. In this paper, we provide a systematical review of PH and PH-based supervised and unsupervised models from a computational perspective. Our emphasizes are the recent development of mathematical models and tools, including PH softwares and PH-based functions, feature representations, kernels, and similarity models. Essentially, this paper can work as a roadmap for the practical application of PH-based machine learning tools. Further, we consider different topological feature representations in different machine learning models, and investigate their impacts on the protein secondary structure classification.

Keywords: Persistent homology, machine learning, persistent diagram, persistent barcode, kernel, feature extraction

1. Introduction

Machine learning models have achieved tremendous success in computer vision, speech recognition, image analysis, text analysis, etc. However, their application in high-dimensional complicated systems have been hindered significantly by proper feature representations. Mathematically, features from geometric analysis can characterize the local structure information very well, but tend to be inundated with details and will result in data complexity. Features generated from traditional topological models, on the other hand, preserve the global intrinsic structure information, but they tend to reduce too much structure information and are rarely used in quantitative characteriza-

*The first two authors contribute equally.

tion. Recently, persistent homology (PH) has been developed as a new multiscale representation of topological features (Edelsbrunner et al., 2002; Zomorodian and Carlsson, 2005, 2008). It is able to bridge the gap between geometry and topology, and open up new opportunities for researchers from mathematics, computer sciences, computational biology, biomathematics, engineering, etc. The essential idea of PH is to employ a filtration procedure, so that each topological generator is equipped with a geometric measurement. In this filtration process, a series of nested simplicial complexes encoded with structural topological information from different scales are produced. The intrinsic topological properties can be evaluated. It is found that some topological invariants “live” longer in these simplicial complexes, whereas others “die” quickly when filtration value changes. The “lifespans” or “persisting times” of these invariants are directly related to geometric properties (Dey et al., 2008; Dey and Wang, 2013; Mischaikow and Nanda, 2013). Simply speaking, long-lived Betti numbers usually represent large-sized features. In this way, topological invariants can be quantified by their persistence in the filtration process. In other words, their lifespans or persisting times give a relative geometric measurement of the associated topological properties. PH provides a very promising way of structure representation, and has been applied to various fields, including shape recognition (Di Fabio and Landi, 2011), network structure (Silva and Ghrist, 2005; Lee et al., 2012; Horak et al., 2009), image analysis (Carlsson et al., 2008; Pachauri et al., 2011b; Singh et al., 2008; Bendich et al., 2010; Frosini and Landi, 2013), data analysis (Carlsson, 2009; Niyogi et al., 2011a; Wang et al., 2011; Rieck et al., 2012; Liu et al., 2012), chaotic dynamics verification (Mischaikow et al., 1999), computer vision (Singh et al., 2008), computational biology (Kasson et al., 2007; Yao et al., 2009; Gameiro et al., 2013; Xia and Wei, 2014; Xia et al., 2015a; Wang and Wei, 2016; Xia and Wei, 2015b,a), amorphous material structures (Hiraoka et al., 2016; Saadatfar et al., 2017), etc. Various softwares, including JavaPlex (Tausz et al., 2011), Perseus (Nanda), Dipha (Bauer et al., 2014a), Dionysus (Dio), jHoles (Binchi et al., 2014), GUDHI (Maria, 2015), Ripser (Bauer, 2017), PHAT (Bauer et al., 2014c), DIPHA (Bauer et al., 2014b), R-TDA package (Fasy et al., 2014), etc. have been developed. The results from PH can be visualized by many methods, including persistent diagram (PD) (Mischaikow and Nanda, 2013), persistent barcode (PB) (Ghrist, 2008b), persistent landscape (Bubenik and Kim, 2007; Bubenik, 2015), persistent image (Adams et al., 2017), etc. When structures are symmetric or have unique topological properties, topological fingerprints can be obtained from the PH analysis and further used in the quantitative characterization of their structures and functions (Xia and Wei, 2014; Xia et al., 2015a; Xia, 2018). However, when the systems get more complicated, it becomes more challenging to directly build models on the PB or PD. Instead, machine learning models can be employed to extract the important information or to learn from these topological features.

The persistent-homology-based machine learning (PHML) models have been used in various areas, including image analysis (Bae et al., 2017; Han et al., 2016; Qaiser et al., 2018; Makarenko et al., 2016; Obayashi et al., 2018; Giansiracusa et al., 2017), shape analysis (Bonis et al., 2016; Zhou et al., 2017; Li et al., 2014; Guo et al., 2018; Zeppelzauer et al., 2018), time-series data analysis (Seversky et al., 2016; Anirudh et al., 2016a; Zhang et al., 2015; Wang et al., 2014; Umeda, 2017), computational biology (Pachauri et al., 2011a; Dey and Mandal, 2018; Cang et al., 2015), noise data (Niyogi et al., 2011b), sphere packing (Robins and Turner, 2016), language analysis (Zhu, 2013), etc. Especially, topological-based machine learning has achieved remarkable success in drug design (Cang and Wei, 2017c,b; Nguyen et al., 2017; Cang and Wei, 2017a; Cang et al., 2018; Wu and Wei, 2018). They have delivered the best results in 10 out of the 26 competitive tasks of D3R Grand Challenges (Nguyen et al., 2018), which is widely regarded as the most difficult challenge in drug design. The huge success shows that, with the proper topological simplification, specially-designed PH models can not only preserve the critical chemical and biological information, but also enables an efficient topological description of biomolecular interactions (Cang et al., 2018). However, unlike geometric and traditional topological models, several problems exist in PHML models, including the construction and generation of meaningful metrics, kernels, and feature vectors.

The unique format of PH outcomes poses a great challenge for a meaningful metrics. To solve this problem, distance measurements or metrics (Mileyko et al., 2011; Turner et al., 2014; Chazal et al., 2017; Carriere and Bauer, 2018; Anirudh et al., 2016b) has been considered, including Gromov-Hausdorff distance, Wasserstein distance (Mileyko et al., 2011), bottleneck distance (Mileyko et al., 2011), probability-measure-based distance (Chazal et al., 2011; Marchese and Maroulas, 2017; Chazal et al., 2017), Fisher information metric (Anirudh et al., 2016b). These metric definitions are usually based on PD, which can be considered as a two dimensional point distribution. However, unlike common point cloud data, PD points have different topological significance. A PD point closed to diagonal line, meaning its death time is only slightly larger than its birth time, is usually regarded as less “useful” than the ones that are far away from the diagonal line. Because short persisting times indicate “insignificant” topological features or “noise”. Although this is not true in various physical, chemical and biological data, in which short-lived invariants have important physical meanings (such as bond lengths, benzene ring size, etc), intrinsic topological features are associated the long-lived topological generators. Given these considerations, pseudo points are introduced and placed on the diagonal lines to guarantee the same number of points in two PDs for comparison. Further, the Wasserstein distance is used to measure the best possible matching from one PD to the other, and bottleneck distance is just a special type of Wasserstein distance. It is found that under Wasserstein metric, PDs is complete and separable (Mileyko et al., 2011). Fréchet means and variances, which are generalization of mean and variance to a general metric space, can also be defined on PDs (Turner et al., 2014) and further enable a probabilistic analysis of PDs. In Wasserstein distance, cardinality difference between two PDs is not explicitly penalized, instead the unmatched points from the two PDs are penalized by their distance to the PD diagonal lines. A probability-measure-based distance function is proposed (Chazal et al., 2011; Marchese and Maroulas, 2017; Chazal et al., 2017) to account for changes in small persistence and cardinality. It also enables statistical structure in the form of Fréchet means and variances and establishes a classification scheme. Once PDs are transformed into probability density functions, Fisher information metric (FIM) can also be used to evaluate the distance between PDs (Anirudh et al., 2016b). All these distance measurements and metrics can be used in kernel constructions, and further used in machine learning models.

With the significant role of kernels in machine learning models, various PH-based kernels have been proposed, including persistence scale space (PSS) kernel (Reininghaus et al., 2015), universal persistence scale space (u-PSS) kernel (Kwitt et al., 2015) persistence weighted Gaussian (PWG) kernel (Kusano et al., 2016), sliced Wasserstein (SW) kernel (Carriere et al., 2017), persistence Fisher (PF) kernel (Le and Yamada, 2018), geodesic topological kernels (Padellini and Brutti, 2017), etc (Chazal et al., 2017; Carriere and Bauer, 2018). Constructed from PDs/PBs, these kernels can be directly incorporated into kernel-based machine learning methods, including kernel perception, kernel support vector machine, principal components analysis, spectral clustering, Gaussian process, etc. In PSS kernel, points in a PD together with its counterparts, which are generated by flipping the points in the PD along the diagonal line, are associated or convolution with Gaussian kernels. A tunable scale parameter is incorporated into these Gaussian kernels, thus for each PD, a multiscale function is generated. The PSS kernel is defined as the inner product of the multiscale functions. Further, the u-PSS kernel is a generalization of PSS, so that it satisfies the universal property. The PWG kernel is designed to attenuate the influence from the short-lived topological generators, which are generally considered as noise. Computationally, random Fourier features can be employed to increase the efficiency of calculating PWG kernel. In SW kernel, points in PDs are projected on to lines passing through the origin. By systematically varying the slopes of these lines, the distance between two PDs is transformed into the measurement of distances between their projected points on these lines. In PF kernel, each PD is transformed into a normalized probability density function, of which the square-root forms a unit Hilbert sphere. Based on the Hilbert sphere space, the Fisher information metric (FIM) can be used to define an inner product metric and a kernel is generated by incorporating the FIM into an exponential function. In a geodesic topological kernel, Wasserstein distance is directly incorporated into an exponential function. However, the geodesic

topological kernels are not positive definite. PH-based kernels are one way to combine topological information with machine learning models, another important way is to generate unique vectors made of topological features and use them in machine learning models.

Topological features can be extracted from PDs/PBs. The simplest way of PD/PB-based feature generation is to collect their statistical properties, such as the sum, mean, variance, maximum, minimum, etc (Cang et al., 2015). Special topological properties, such as the total Betti number in a certain filtration value, can also be considered as features (Cang et al., 2015). Further, a set of coordinates, which reflect properties of the corresponding ring of functions, are proposed as the topological features in digit number classification (Adcock et al., 2016). Tropical coordinates on the space of barcodes, which are stable with respect to Wasserstein distances, are also important topological features (Kališnik, 2018). However, all these methods use only partial information from PB. A more systematical way of constructing topological feature vectors from PDs/PBs is the binning approach (Cang and Wei, 2017c; Cang et al., 2018). The essential idea is to discrete the PB or PB into various elements, which are then concatenated into a feature vector. More specifically, for PB, the filtration time can be subdivided into equally-sized bins. The persistent Betti numbers in these bins form a vector. Similarly, for PDs, the binning of the birth and death time will subdivided them into a equally-sized mesh. The number of topological generators in each grid box is an element of the topological feature vector. Mathematically, binning is just to employ a Cartesian grid discretization, which is simplest way to discretize a computational domain. Recently, a new way of feature representation, known as persistent codebooks, has been proposed (Zielinski et al., 2018; Bonis et al., 2016). In these models, a fixed-sized vector representation of PDs is achieved by clustering and bag of words quantization methods, including bag of words encoding, vector of locally aggregated descriptor, and Fisher vector. Further, instead of generating features directly from PDs/PBs, another type of feature construction is to construct persistent functions, discretize them into elements and concatenate them into a vector (Bubenik and Dłotko, 2017; Adams et al., 2017). These persistent functions includes persistent Betti number, persistent Betti function (Xia et al., 2018), persistent landscape (Bubenik and Dłotko, 2017), persistent surface (Adams et al., 2017), etc. Similar to the binning approach, these functions are discretized first and then concatenated into a feature vector. Moreover, recently an image representation of PDs/PBs has been found extremely useful in drug design (Cang and Wei, 2017c; Cang et al., 2018). In this model, biomolecular structure has been decomposed into element-specific models, each of which has its feature vector from binning approach. Instead of using these feature vectors directly, an image representation is proposed by stacking all these feature vectors together systematically. This image representation is essentially a multidimensional persistence and can be generalized to three dimensional volumetric data. More importantly, the input of topological features as images suits perfectly with the convolutional neural network (CNN) model. In this way, it really brings out the great power of persistence representation. Finally, a persistent path and signature feature model has been proposed (Chevyrev et al., 2018). In this model, the barcode information is embedded into a persistent path. And the persistent path is further transformed into tensor series, which can be represented into a feature vector. It is worth mentioning that for PHML models, a great promise comes from new ways of topological representations that can incorporate more structure information, including persistent local homology (Bendich et al., 2015; Fasy and Wang, 2016; Bendich et al., 2007, 2012; Ahmed et al., 2014), element specific PH (Cang and Wei, 2017b,a,c; Cang et al., 2018; Wu and Wei, 2018), weighted PH (Ren et al., 2017; Wu et al., 2018), multidimensional PH (Carlsson and Zomorodian, 2009; Carlsson et al., 2009; Cohen-Steiner et al., 2006; Cerri and Landi, 2013; Xia and Wei, 2015b; Xia et al., 2015b), etc. From the statistical perspective, when a large-scale feature vector is used to represent the topological features from PBs/PDs, the PHML models will also suffer from the curse of dimensionality. In this situation, techniques for variable selection and regularization should be considered, such as the high-dimensional statistical tools used in different fields: (Fan et al., 2008; Cai and Liu, 2011; Pun and Wong, 2018, 2016; Chiu et al., 2017; Pun, 2018; Hadimaja and Pun, 2018) and the dropout approach in neural networks (Srivastava et al., 2014), etc.

In this paper, we review the persistent-homology-based machine learning (PHML) models and discuss its application in protein structure classification. Our focus is to provide a general guidance, as demonstrated in Figure 1, for the practical application of topology-aware machine learning models. We also deliver a systematical study of PH-based metrics, kernels, and feature vectors. The comparison and analysis of these methods will help to generate more robust and efficient algorithms and models. In application part, we discuss the combination of different topological feature selections with machine learning models.

The remainder of this paper is organized as follows. Section 2 is a general pipeline for the PHML models. A more detailed discussion of the fundamentals of PH is presented in Section 3. Section 4 is devoted for PH-based functions, metrics, kernels, and feature vectors, and the construction of PH-based unsupervised learning and supervised learning. We test the feature selection and its relation with different machine learning models by a protein classification example in Section 5. The paper ends with a conclusion.

2. General Pipeline for Persistent-Homology-based Machine Learning

The essential idea for PHML is to extract topological features from the data using PH, and then combine these features with machine learning methods, including both supervised learning and unsupervised learning approaches. As illustrated in Figure 1, PHML in computation can be divided into four steps, i.e., simplicial complex construction, PH analysis, topological feature extraction and topology-based machine learning.

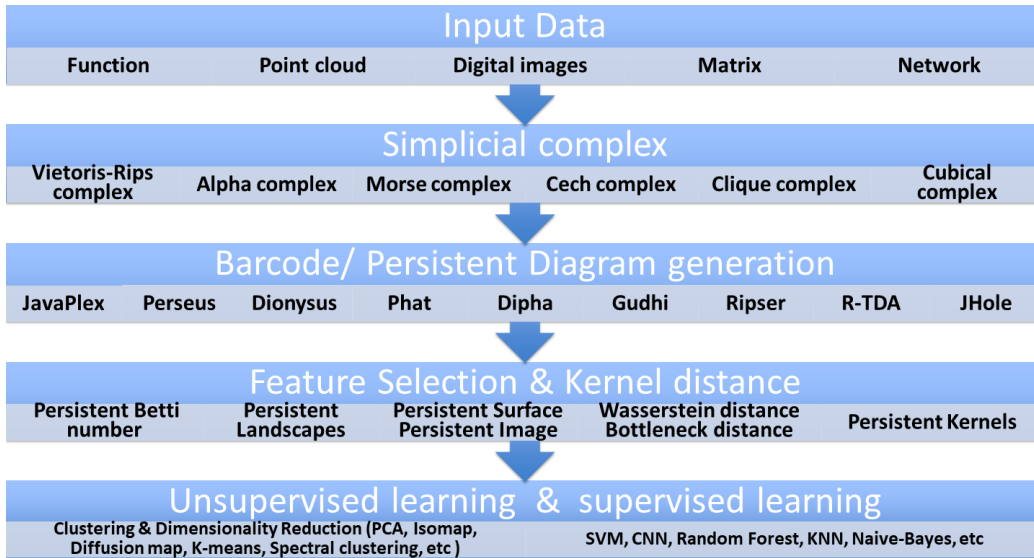


Figure 1: The flowchart for PHML modeling. For different data types, different simplicial complexes are considered. With a suitable filtration parameter, PH analysis can be implemented by designed softwares. The result from the PH is transformed into feature vectors, distance measurements or special kernels, which are further combined with supervised or unsupervised methods from machine learning.

The first step is to construct simplicial complex (or complexes) from the studied data. In topological modeling, we may have various types of data, including functional data, point cloud data, matrixes, networks, images, etc. These data need to be represented by suitable simplicial complexes. Roughly speaking, the simplicial complex can be viewed as a set of combinatorial elements generated from the discretization of spaces. Cartesian grids and triangular meshes can be viewed

as two dimensional simplicial complexes. Depending on the type of studied data, different simplex models can be considered, including Vietories-Rips complex, *Cech* complex, Alpha complex, Morse complex, cubical complex, clique complex, CW complex, etc. The detailed explanation of simplicial complexes will be given in Section 3.1.

The second step is the PH analysis. PH is a newly-invented model deeply-rooted in algebraic topology, computational topology and combinatorial topology. In PH (Edelsbrunner et al., 2002; Zomorodian and Carlsson, 2005; Carlsson, 2009; Edelsbrunner and Harer, 2010; Zomorodian, 2005), algebraic tools, such as quotient group, homology, exact sequence, etc, are used to characterize topological invariants, including connected components, circles, rings, channels, cavities, voids, etc. Unlike traditional topological models, which capture only the intrinsic structure information and tend to ignore all geometric details, PH works as a multiscale topological representation and enables to embed geometric information back into topological invariants. This is achieved through a new idea called filtration (see Figure 3 for details). With a suitable filtration process, the persistence of topological invariants can be calculated. Roughly speaking, the persistence tells you the geometric size of the invariant. Different softwares are currently available for PH analysis of different data structures (see Figure 4 for details).

The third step is to extract meaningful topological features from PH results. The PH results are usually represented as PBs or PDs (see Figure 5 for details). Neither of these representations can be used directly as input for machine learning models. Therefore, we need to transform the PH results into representations, which can be easily incorporated into machine learning models. Currently, two basic approaches are available. The first one is to generate special PH-based kernels or similarity measurements. These kernels and similarity matrixes can then be combined with PCA, SVM, K-means, spectral clustering, isomap, diffusion map, and other learning models to perform the data classification and clustering. The second one is to generate topological feature vectors from PHA results. Binning approach is the most commonly used approach to discretize the PB or PD into a feature vector. The detailed discussion will be given in Section 4.

The last step is to combine the topological features with machine learning algorithms. Essentially, these features can be used directly used in both unsupervised learning and supervised learning models. Depending on the learning models, we should consider different feature selection and representation models to bring out the best performance of the model.

3. Persistent Homology for Data Modeling and Analysis

This section is devoted to the fundamentals of PH. We present a brief review of simplicial complexes and PH analysis in the first and second parts, respectively. For interested readers, a more detailed description of simplicial complex and PH can be found in papers (Zomorodian and Carlsson, 2005; Edelsbrunner et al., 2002; Kaczynski et al., 2004; Carlsson, 2009; Mischaikow and Nanda, 2013; Edelsbrunner and Harer, 2010).

3.1 Simplicial Complexes

A simplicial complex is a combination of simplexes under certain rules. It can be viewed as a generalization of network or graph model.

3.1.1 ABSTRACT SIMPLICIAL COMPLEX

A simplex is the building block for simplicial complex. It can be viewed as a generalization of a triangle or tetrahedron to their higher dimensional counterparts.

Definition 1 A geometric k -simplex $\sigma^k = \{v_0, v_1, v_2, \dots, v_k\}$ is the convex hull formed by $k + 1$ affinely independent points $v_0, v_1, v_2, \dots, v_k$ in Euclidean space R^d as follows,

$$\sigma^k = \left\{ \lambda_0 v_0 + \lambda_1 v_1 + \dots + \lambda_k v_k \mid \sum_{i=0}^k \lambda_i = 1; 0 \leq \lambda_i \leq 1, i = 0, 1, \dots, k \right\}.$$

A face τ of k -simplex σ^k is the convex hull of a non-empty subset. We denote it as $\tau \leq \sigma^k$

Geometrically, a 0-simplex is a vertex, a 1-simplex is an edge, a 2-simplex is a triangle, and a 3-simplex represents a tetrahedron. An oriented k -simplex $[\sigma^k]$ is a simplex together with an orientation, i.e., ordering of its vertex set. Simplices are the building block for (geometric) simplicial complex.

Definition 2 A geometric simplicial complex K is a finite set of geometric simplices that satisfy two essential conditions:

1. Any face of a simplex from K is also in K .
2. The intersection of any two simplices in K is either empty or shares faces.

The dimension of K is the maximal dimension of its simplices. A geometric simplicial complex K is combinatorial set, not a topological space. However, all the points of R^d that lie in the simplex of K aggregate together to topologize it into a subspace of R^d , known as polyhedron of K .

Graphs and networks, which are comprised of only vertices and edges, can be viewed as a simplicial complex with only 0-simplex and 1-simplex.

Definition 3 An abstract simplicial complex K is a finite set of elements $\{v_0, v_1, v_2, \dots, v_n\}$ called abstract vertices, together with a collection of subsets $(v_{i_0}, v_{i_1}, \dots, v_{i_m})$ called abstract simplices, with the property that any subset of a simplex is still a simplex.

For an abstract simplicial complex K , there exists a geometric simplicial complex K' whose vertices are in one-to-one correspondence with the vertices of K and a subset of vertices being a simplex of K' if and only if they correspond to the vertices of some simplex of K . The geometric simplicial complex K' is called the geometric realization of K .

Based on different data types, there are various ways of defining simplicial complexes. The most commonly used ones are Čech complex, Vietoris-Rips complex, Alpha complex, Clique complex, Cubic complex, Morse complex, etc.

3.1.2 Čech COMPLEX AND VIETORIS-RIPS COMPLEX

Let X be a point set in Euclidean space R^d and \mathcal{U} is a good cover of X , i.e., $X \subseteq \bigcup_{i \in I} U_i$.

Definition 4 The nerve \mathcal{N} of \mathcal{U} is defined by the following two conditions:

1. $\emptyset \in \mathcal{N}$;
2. If $\bigcap_{j \in J} U_j \neq \emptyset$ for $J \subseteq I$, then $J \in \mathcal{N}$.

Theorem 1 (Nerve theorem) The geometric realization of the nerve of \mathcal{U} is homotopy equivalent to the union of sets in \mathcal{U} .

We can define $B(x, \varepsilon)$ to be the closed balls of radius ε centred at $x \in X$, then the union of these balls is a cover of space X and Čech complex is the nerve of this cover.

Definition 5 The Čech complex with parameter ε of X is the nerve of the collection of balls $B(x, \varepsilon)$. The Čech complex $\check{C}_\varepsilon(X)$ can be represented as $\check{C}_\varepsilon(X) := \{\sigma \in X \mid \bigcap_{x \in \sigma} B(x, \varepsilon) \neq \emptyset\}$.

Definition 6 *The Vietoris-Rips complex (Rips complex) with parameter ε denoted by $\mathcal{R}_\varepsilon(X)$, is the set of all $\sigma \subseteq X$, such that the largest Euclidean distance between any of its points is at most 2ε .*

It should be noticed that both Čech complex and Vietoris-Rips complex are abstract simplicial complexes, that are defined on point cloud data in a metric space. And different ε values will usually result in different Čech and Rips complexes. However, only Čech complex preserves the homotopy information of the topological spaces formed by the ε -balls.

3.1.3 ALPHA COMPLEX

Alpha complex is used in computational geometry (Edelsbrunner and Mücke, 1994; Edelsbrunner, 1992; Edelsbrunner and Harer, 2010). It is a set of subcomplexes from the Delaunay triangulation of a point set in R^d .

Definition 7 *Let X be a finite point set in R^d . Voronoi cell of a point x in X is the set of points $V_x \subseteq R^d$ for which x is the closest of the points in X , i.e. $V_x = \{u \in R^d : |u - x| \leq |u - x'|, \forall x' \in X\}$.*

Definition 8 *The Delaunay complex of a finite set $X \in R^d$ is defined as the nerve of the Voronoi diagram.*

We define $R_\varepsilon(x)$ to be the intersection of the Voronoi cell V_x with $B(X, \varepsilon)$, i.e., $R_\varepsilon(x) = V_x \cap B(X, \varepsilon)$ for every $x \in X$.

Definition 9 *The alpha complex $\mathcal{A}_\varepsilon(X)$ is defined as the nerve of the covers formed by $R_\varepsilon(x)$ for every $x \in X$, i.e. $\mathcal{A}_\varepsilon(X) := \{\sigma \in X \mid \bigcap_{x \in \sigma} R_\varepsilon(x) \neq \emptyset\}$.*

The geometric realization of alpha complex $\mathcal{A}_\varepsilon(X)$ is homotopy equivalent to the union of the closed balls $\bigcup_{x \in X} B(X, \varepsilon)$.

3.1.4 CLIQUE COMPLEX

Clique complex, also known as flag complex, is derived from graph and network models (Frohman, 2008; Giusti et al., 2015; Zomorodian, 2010). Its definition is very straightforward. For a graph G , a complete graph is a graph, of which any two vertices are connected by an edge and a clique is a set of vertices that forms a complete subgraph in G . A k -clique complex is formed from a clique with $k + 1$ vertices. Since subsets of cliques are also cliques, the clique complex is a simplicial complex.

Figure 2 illustrate the the comparison between Čech complex, Vietoris-Rips complex, Alpha complex and Clique complex. A point cloud data can be used to generate different simplicial complexes. The construction of the simplicial complex is highly dependent on the physical properties of data and the underlying topological space.

3.1.5 CUBICAL COMPLEX

Image and volumetric data are arguably the important types of data in scientific computing. It is of key importance in computational topology to build up suitable simplicial complexes from these data. Since image and volumetric data is made from pixels and voxels, which are two and three dimensional cubes, it is natural to come up with the idea of cubical complex (Kaczynski et al., 2004).

Definition 10 *An elementary interval is a closed interval $I \subset R$ of the form $I = [l, l+1]$ or $I = [l, l]$, for some $l \in Z$. Here $[l, l]$ is an interval contains only one point. Elementary intervals that consist of a single point are degenerate.*

Definition 11 *An elementary cube Q is a finite product of elementary intervals, that is $Q = I_1 \times I_2 \times \dots \times I_d \subset R^d$, where each I_i is an elementary interval. The set of all elementary cubes in R^d is denoted by \mathcal{K}^d . The set of all elementary cubes is denoted by \mathcal{K} , $\mathcal{K} := \bigcup_{d=1} \mathcal{K}^d$*

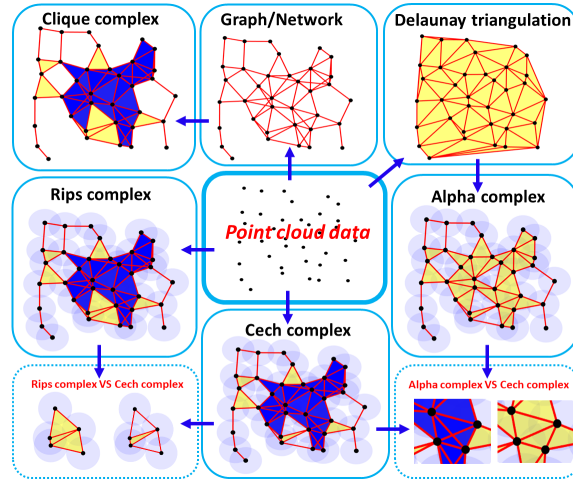


Figure 2: The comparison of Čech complex, Vietoris-Rips complex, Alpha complex and Clique complex. Essentially, Rips and Čech simplexes are different as Rips only requires the “overlapping” of any two vertices to form a simplex. Clique complex is based on cliques that are derived from networks or graphs. Alpha complex is a subset of Delaunay triangulation and only suitable for subjects in Euclidian spaces. Interestingly, the same point cloud data, under different rules, can be used to generated different simplicial complexes, indicating that physical properties of data and its underly topological space is important for the construction of the simplicial complex.

Definition 12 A set $K \subset R^d$ is a cubical complex if K can be written as a finite union of elementary cubes.

3.1.6 CW COMPLEX

CW complex plays an important role in topology and it has more freedom in the shape of the simplex. More specifically, we can define a closed unite ball in d -dimensional Euclidean space as $B^d = \{x \in R^d : |x| \leq 1\}$ and its boundary is the unit $(d - 1)$ -sphere $S^{d-1} = \{x \in R^d : |x| = 1\}$. A d -cell is a topological space which is homomorphic to B^d , i.e., there exist a bijection mapping between d -cell and B^d . Roughly speaking, a cell can be viewed as a simplex with more complicated shape. The boundary of d -cell is a $(d - 1)$ -cell and a CW complex is formed when these cells satisfied the two basic conditions as in Definition 2.

Definition 13 A finite CW complex is any topological space X such that there exists a finite nested sequence $\emptyset \subset X^0 \subseteq X^1 \subseteq \dots \subseteq X^n = X$ such that for each $i = 0, 1, 2, \dots, n$, X_i is the results of attaching a cell to X_{i-1} . The sequence above is called the CW decomposition of X .

3.1.7 MORSE-SMALE COMPLEX

The Morse-Smale complex is a special kind of CW complex. Morse-Smale complex is defined usually on a manifold. It explores the manifold properties through a specially-designed function on it.

Definition 14 Let f be a C^2 continuous function on a manifold \mathbb{M} . A point $p \in \mathbb{M}$ is a critical point if its derivatives with respect to a local coordinate system on \mathbb{M} vanish.

Morse theory studies the non-degenerate critical points, known as Morse points. Usually, the topological property of the critical points can be derived from their Hessian matrix,

$$H(f) = \begin{bmatrix} \frac{\partial f}{\partial x_1^2} & \frac{\partial f}{\partial x_1 \partial x_2} & \cdots & \frac{\partial f}{\partial x_1 \partial x_n} \\ \frac{\partial f}{\partial x_2 \partial x_1} & \frac{\partial f}{\partial x_2^2} & \cdots & \frac{\partial f}{\partial x_2 \partial x_n} \\ \vdots & \vdots & \ddots & \vdots \\ \frac{\partial f}{\partial x_n \partial x_1} & \frac{\partial f}{\partial x_n \partial x_2} & \cdots & \frac{\partial f}{\partial x_n^2} \end{bmatrix}.$$

Let $\lambda_1 \leq \lambda_2 \leq \dots \leq \lambda_n$ be the eigenvalues of $H(f)$. A critical point is degenerate when one of the eigenvalues equals to zero, otherwise it is non-degenerate. For non-degenerate critical point, its number of negative eigenvalues is defined as the index of this critical point. This index is highly related to the topology of the manifold.

Lemma 1.1 (*Morse Lemma*) *Let p be a non-degenerate critical point of f with index λ and let $c = f(p)$, there exists a local coordinate system $y = (y_1, y_2, \dots, y_n)$ in a neighborhood of p with p as its origin and $f(y) = c - y_1^2 - y_2^2 - \dots - y_\lambda^2 + y_{\lambda+1}^2 + y_{\lambda+2}^2 + \dots + y_n^2$.*

Definition 15 *Morse function is a smooth function on a manifold, such that all critical points are non-degenerate, and the critical points have distinct function values.*

Based on the Morse function, the gradient flow can be calculated and used to decompose a manifold. More specifically, at a point p in \mathbb{M} , we can define its tangent plane as $T_p(\mathbb{M})$, γ as any curve passing through it, and tangent vector as $v_p \in T_p(\mathbb{M})$ with v the velocity of curve γ . We can explore how a Morse function changes in the direction specified by the tangent vector.

Mathematically, for a curve $\gamma(s)$ passing through p and tangent to $v_p \in T_p(\mathbb{M})$, the gradient ∇f of a Morse function f along this curve is $\frac{d\gamma}{ds} \cdot \nabla f = \frac{d(f(\gamma))}{ds}$.

Definition 16 *An integral line $\gamma(s) : R \rightarrow \mathbb{M}$ is a maximal path whose tangent vectors agree with the gradient, i.e., $\frac{\partial}{\partial s} \gamma(s) = \nabla f(\gamma(s))$ for all $s \in R$. We call $\text{org}\gamma = \lim_{s \rightarrow -\infty} \gamma(s)$ the origin and $\text{dest}\gamma = \lim_{s \rightarrow +\infty} \gamma(s)$ the destination of the path γ . Integral lines have the following properties. First, two integral lines are either disjoint or the same. Second, the integral lines cover all of \mathbb{M} . Third, the limits $\text{org}\gamma$ and $\text{dest}\gamma$ are critical points of f .*

Definition 17 *The stable manifold $S(p)$ and the unstable manifold $U(p)$ of a critical point p are defined as $S(p) = \{p\} \cup \{x \in \mathbb{M} \mid x \in \text{im}\gamma, \text{dest}\gamma = p\}$ and $U(p) = \{p\} \cup \{x \in \mathbb{M} \mid x \in \text{im}\gamma, \text{org}\gamma = p\}$, respectively, where $\text{im}\gamma$ is the image of the path $\gamma \in \mathbb{M}$.*

Both sets of manifolds decompose \mathbb{M} into open cells.

Definition 18 *The stable manifold $S(p)$ of a critical point p with index $i = i(p)$ is an open cell of dimension $\dim S(p) = i$.*

A Morse function is a Morse-Smale function if the stable and unstable manifolds intersect only transversally.

Definition 19 (*Morse-Smale complex*) *Connected components of sets $U(p_i) \cap S(p_j)$ for all critical points $p_i, p_j \in \mathbb{M}$ are Morse-Smale cells. We refer to the cells of dimension 0, 1, and 2 as vertices, arcs, and regions, respectively. The collection of Morse-Smale cells form a complex, the Morse-Smale complex.*

3.2 Persistent Homology Analysis

3.2.1 HOMOMOLOGY

Definition 20 An orientation of a k -simplex $\sigma^k = \{v_0, v_1, v_2, \dots, v_{k+1}\}$ is an equivalence class of orderings of the vertices of σ^k , where $(v_0, v_1, v_2, \dots, v_{k+1}) \sim (v_{\tau(0)}, v_{\tau(1)}, v_{\tau(2)}, \dots, v_{\tau(k+1)})$ are equivalent orderings if the parity of the permutation τ is even. We denote an oriented simplex by $[\sigma^k] = [v_0, v_1, v_2, \dots, v_{k+1}]$.

Definition 21 A k -th chain group $C_k(K)$ of a simplicial complex K is an Abelian group made from all k -chains from the simplicial complex K together with addition operation.

A linear combination of k -simplexes forms a k -chain c , i.e., $c = \sum_i \alpha_i \sigma_i^k$. In computational topology, we usually assume $\{\alpha_i \in \mathbb{Z}_2\}$. All k -chains from the simplicial complex K together with addition operation (modulo-2) will form an Abelian group $C_k(K, \mathbb{Z}_2)$. Homomorphism can be defined between these Abelian groups.

Definition 22 The boundary operator $\partial_k : C_k \rightarrow C_{k-1}$ of an oriented k -simplex $[\sigma^k] = [v_0, v_1, v_2, \dots, v_k]$ can be denoted as $\partial_k[\sigma^k] = \sum_{i=0}^k [v_0, v_1, v_2, \dots, \hat{v}_i, \dots, v_k]$. Here $[v_0, v_1, v_2, \dots, \hat{v}_i, \dots, v_k]$ means a $(k-1)$ oriented simplex, which is generated by the original set of vertices $v_0, v_1, v_2, \dots, v_{i-1}, v_{i+1}, \dots, v_k$ except v_i .

The boundary operator satisfies several properties, including $\partial_0 = 0$ and $\partial_{k-1}\partial_k = 0$. With the boundary operation, we can define the k -th cycle group Z_k and the k -th boundary group B_k as

$$Z_k = \text{Ker } \partial_k = \{c \in C_k \mid \partial_k c = 0\}, \quad B_k = \text{Im } \partial_{k+1} = \{c \in C_k \mid \exists d \in C_{k+1} : c = \partial_{k+1} d\}.$$

Since $\partial_{k-1}\partial_k = 0$, cycle and boundary groups satisfy $B_k \subseteq Z_k$.

Definition 23 The k -th homology group is the quotient group $H_k = Z_k/B_k$. The rank of k -th homology group H_k is called k -th Betti number and satisfies $\beta_k = \text{rank } H_k = \text{rank } Z_k - \text{rank } B_k$.

Geometrically, we can regard β_0 as the number of isolated components, β_1 the number of one-dimensional loops, circles, or tunnels and β_2 the number of two-dimensional voids or holes.

3.2.2 PERSISTENT HOMOMOLOGY

The essence of PH is its filtration process, during which a series of topological spaces in different scales are generated (see Figure 3).

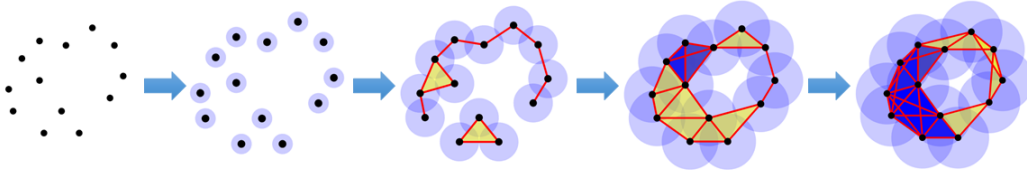


Figure 3: The illustration of a filtration process in PH. Each point is associated with a same-sized sphere. And the sphere radius is used as the filtration parameter. With the enlargement of the radius size, a series of nested simplicial complexes are generated.

Definition 24 A filtration of a simplicial complex K is a nested sequence of subcomplexes, $\emptyset \subset K^0 \subseteq K^1 \subseteq \dots \subseteq K^n = K$. We call a simplicial complex K with a filtration a filtered complex.

Definition 25 Let K^l be a filtration of a simplicial complex K , and the $Z_k^l = Z_k(K^l)$ and $B_k^l = B_k(K^l)$ be the k -th cycle and boundary group of K^l , respectively. The k -th homology group of K^l is $H_k^l = Z_k^l/B_k^l$. The k -th Betti number β_k^l of K^l is the rank of H_k^l .

Definition 26 The p -persistent k -th homology group at filtration time l can be represented as

$$H_k^{l,p} = Z_k^l / (B_k^{l+p} \cap Z_k^l).$$

The p -persistent k -th Betti number $\beta_k^{l,p}$ of K^l is the rank of $H_k^{l,p}$.

Essentially, persistence gives a geometric measurement of the topological invariant.

Softwares for PH Various softwares, including JavaPlex (Tausz et al., 2011), Perseus (Nanda), Dipha (Bauer et al., 2014a), Dionysus (Dio), jHoles (Binchi et al., 2014), GUDHI (Maria, 2015), Ripser (Bauer, 2017), PHAT (Bauer et al., 2014c), DIPHA (Bauer et al., 2014b), R-TDA package (Fasy et al., 2014), etc, have been developed. These softwares are based on different types of simplicial complexes and can be used to process different types of data (see Figure 4).

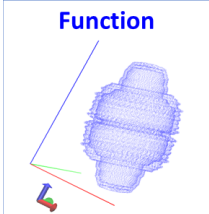
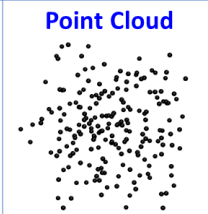
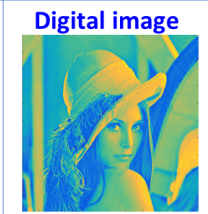
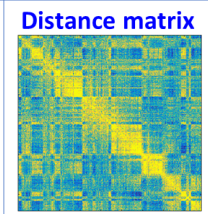

| Function | Point Cloud | Digital image | Distance matrix | Network |
|---|---|---|---|---|
|  |  |  |  |  |
| Morse, Cubical | Rips, Alpha | Morse, Cubical | Rips, Clique | Rips, Clique |
| PERSEUS (Morse), PHAT (Morse), Dipha (Morse), GUDHI (Morse), R-TAD (Morse) | JAVAPLEX (Rips), PERSEUS (Rips), PHAT (Rips), Dipha (Rips), GUDHI (Rips), R-TAD (Rips, Alpha), DIONYSUS (Rips, Alpha) | PERSEUS (Morse), PHAT (Morse), Dipha (Morse), GUDHI (Morse), R-TAD (Morse) | JAVAPLEX (Rips), PERSEUS (Rips), PHAT (Rips), Dipha (Rips), GUDHI (Rips), R-TAD (Rips, Alpha), DIONYSUS (Rips), jHoles (Clique) | JAVAPLEX (Rips), PERSEUS (Rips), PHAT (Rips), Dipha (Rips), GUDHI (Rips), R-TAD (Rips, Alpha), DIONYSUS (Rips), jHoles (Clique) |

Figure 4: The illustration of the simplicial complexes and PH softwares for different types of data. Depending on the data types, different simplicial complexes should be used to capture the intrinsic topology of the data. For instance, Rips complex can be used for point cloud data. With a suitable filtration parameter, PH can be further employed to extract the multiscale topological information. Various softwares are available for PH analysis.

Persistent barcodes and persistent diagram The results from PH can be represented as pairs of birth times (BTs) and death time (DTs). More specifically, for each generator (topological invariant), BT and DT represent the filtration value at which the generator is born and vanished, respectively. They always come in pairs and can be denoted as

$$l_j^k = \{a_j^k, b_j^k\} \text{ with } k \in \mathbb{N} \text{ and } j \in \{1, 2, \dots, N_k\}.$$

We use a_j^k , b_j^k , l_j^k to represent BT, DT, persistence for the j -th topological generator of the k -th dimensional Betti number, respectively. Parameter N_k is the total number of k -th dimensional topological generators. Moreover, dimension number k is always a nonnegative integer (i.e., $k \in \mathbb{N}$). These notations will be consistently used in the following sections unless stated otherwise. To avoid repetition, we will omit the definition of domain for the dimension parameter k and always assume it to be $k \in \mathbb{N}$. For simplification, we also define the set of k -th dimensional barcodes as,

$$L_k = \{l_j^k = \{a_j^k, b_j^k\}_{j \in \{1, 2, \dots, N_k\}}\}.$$

The topological persistence is usually represented in two ways, i.e., persistent barcode (PB) (Ghrist, 2008a) and persistent diagram (PD) (Mischaikow and Nanda, 2013). In PB, each l_j^k is treated as a bar, i.e., the line $[l_j^k] = [a_j^k, b_j^k]$. In PD, each l_j^k is considered as a 2D point with coordinate $\vec{l}_j^k = (a_j^k, b_j^k)$. The upper panel of Figure 5 illustrates the PB and PD for a protein structure with PDB ID: 2BBR. The rotated PD is also widely used. The essential idea is to employ a rotational function $T(x, y) = (x, y - x)$ on the data points in PD. In this way, a point (a_j^k, b_j^k) in PD (a_j^k, b_j^k) , becomes $T(\vec{l}_j^k) = (a_j^k, b_j^k - a_j^k)$ after rotation. The rotated PD is denoted as

$$T(L_k) = \{T(\vec{l}_j^k) = (a_j^k, b_j^k - a_j^k)_{j \in \{1, 2, \dots, N_k\}}\}.$$

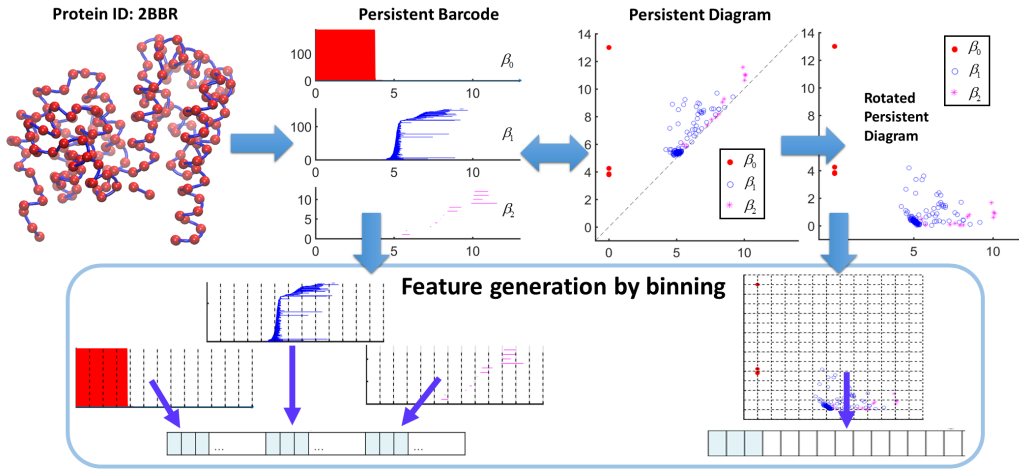


Figure 5: The illustration of the topological feature generation by binning approach. Essentially, binning is to discretize the PBs/PDs into equally-sized elements, count the corresponding Betti numbers (as in PB) or PD points, and concatenate them into a feature vector. The feature vector can then be used in machine learning models.

Persistent local homology A closely related model, the persistent local homology (Bendich et al., 2007, 2012; Ahmed et al., 2014; Bendich et al., 2015; Fasy and Wang, 2016), is proposed based on the algebraic topological concept called local homology groups (Munkres, 2018). Generally speaking, local homology is used to evaluate the local structure of a topological space. If the topological space is topological manifold, the local homology groups for each point are the same. More specifically, we can let X be a topological space embedded in R^d . For a fixed point $p \in R^d$, we can define a ball center at p with radius ϵ $B(p, \epsilon) = \{x \in R^d : |x| \leq 1\}$. The k -th local homology group of X with center point p and radius ϵ is denoted as $LH_k(X, p, \epsilon) = H_k(X \cap B(p, \epsilon))$. Persistent local homology can be used in dimension reduction and manifold dimension detection.

3.2.3 PERSISTENT FUNCTIONS

Based on PB/PD results, different functions are proposed to represent or analyze the topological information (Carlsson, 2009; Bubenik, 2015; Chintakunta et al., 2015). They can be treated as functional data for subsequent analysis (Ramsay and Silverman, 1997; Horváth and Kokoszka, 2012) or used to deduce the structured features as shown in Section 4.1.3-4.1.6 below.

Definition 27 *The persistent Betti number (PBN) or Betti curve is defined as the summation of all the k -th dimensional barcodes,*

$$f(x; L_k) = \sum_j \chi_{[a_j^k, b_j^k]}(x)$$

Function $\chi_{[a_j^k, b_j^k]}(x)$ is a step function, which equals to one in the region $[a_j^k, b_j^k]$ and zero otherwise.

This equation transforms all the k -dimensional barcodes into a one-dimensional function. However, the persistent Betti number is not continuous.

Definition 28 *A continuous persistent Betti function is proposed as follows,*

$$f(x; L_k) = \sum_j e^{-\left(\frac{x - \frac{a_j^k + b_j^k}{2}}{w_j(b_j^k - a_j^k)}\right)^2},$$

where w_j are weight values, which can be adjusted based on different purposes (Xia, 2017).

Another way to represent the barcode result is persistence landscapes (Bubenik, 2015).

Definition 29 *A piecewise linear function can be defined on each individual barcode $\{l_j^k\}$,*

$$f(x, l_j^k) = \begin{cases} 0 & \text{if } x \notin (a_j^k, b_j^k); \\ x - a_j^k & \text{if } x \in (a_j^k, \frac{a_j^k + b_j^k}{2}]; \\ -x + b_j^k & \text{if } x \in [\frac{a_j^k + b_j^k}{2}, b_j^k). \end{cases}$$

The persistence landscape of k -dimensional barcode L_k is the sequence functions $\lambda_m : R \rightarrow [0, \infty]$, $m = 1, 2, 3, \dots$, where $\lambda_m(x)$ is the m -th largest value of $\{f(x, l_j^k)\}_{j=1}^{N_k}$. We set $\lambda_m(x) = 0$ if the m -th largest value does not exist.

Recently, persistent image has been proposed to represent PDs (Adams et al., 2017). The persistent image is derived from persistent surface function.

Definition 30 *The persistent surface for k -th dimensional barcodes L_k is defined as*

$$\rho(x, y, L_k) = \sum_j w(x, y, t_1, t_2) \phi(x, y, l_j^k),$$

where the differentiable probability distribution function $\phi(x, y, l_j^k) = \frac{1}{2\pi\sigma^2} e^{-((x-a_j^k)^2 + (y-(b_j^k-a_j^k))^2)/2\sigma^2}$ and the weight function with two constants t_1 and t_2 is

$$w(x, y, t_1, t_2) = \begin{cases} 0 & \text{if } y \leq t_1; \\ \frac{y-t_1}{t_2-t_1} & \text{if } t_1 < y < t_2; \\ 1 & \text{if } y \geq t_2. \end{cases}$$

The persistent surface can be discretized by a Cartesian grid into image data. By the integration of persistent surface function over each grid (or pixel), a persistent image function is obtained.

To measure the disorder of a system, persistent entropy has been proposed (Merelli et al., 2015; Chintakunta et al., 2015; Rucco et al., 2016; Xia et al., 2018).

Definition 31 *Persistent entropy is defined as*

$$S_k = \sum_j -p_j^k \ln(p_j^k)$$

with the probability function $p_j^k = \frac{b_j^k - a_j^k}{\sum_j (b_j^k - a_j^k)}$.

4. Persistent-Homology-based Machine Learning Methods

4.1 Feature Extraction from PBs/PDs

The topological information within PBs/PDs needs to be converted to (structured) features, so that they can be inputted in machine learning algorithms. These features are usually represented as a quantitative vector. In this section, we summarize the common approaches of feature extraction from PBs/PDs.

4.1.1 BARCODE STATISTICS

The simplest way of feature generation is to collect the statistic measurement of the barcode properties, such as birth times (BTs), death times (DTs) and persistent lengths (PLs). These statistic measurements can be maximal, minimal, mean, variance, summation, among others. In the subsequent experiments, we refer to the 13 barcode statistics in (Cang et al., 2015), which are used to characterize topological structure information. For instance, first/second/third longest Betti-0/Betti-1/Betti-2 PLs, BT/DT for the longest Betti-1/Betti-2; number of Betti-1 bars located at filtration distance $[4.5, 5.5]$ Å, etc.

4.1.2 ALGEBRAIC FUNCTIONS AND TROPICAL FUNCTIONS

Algebraic combinations were also considered (Adcock et al., 2016). For instance, $\sum_j a_j^k (b_j^k - a_j^k)/N_k$, $(\max_j \{b_j^k\} - b_j^k)(b_j^k - a_j^k)/N_k$, $(a_j^k)^2 (b_j^k - a_j^k)^4$, $(\max_j \{b_j^k\} - b_j^k)^2 (b_j^k - a_j^k)^4/N_k$. The average over each bar to eliminate the effects of large variations.

An alternative is to consider the min-plus and max-plus type coordinates (Kališnik, 2018). For instance, $\max_j \{b_j^k - a_j^k\}$, $\max_{i < j} \{(b_i^k - a_i^k) + (b_j^k - a_j^k)\}$, $\max_{i < j < m} \{(b_i^k - a_i^k) + (b_j^k - a_j^k) + (b_m^k - a_m^k)\}$, $\max_{i < j < m < n} \{(b_i^k - a_i^k) + (b_j^k - a_j^k) + (b_m^k - a_m^k) + (b_n^k - a_n^k)\}$, $\sum_j \{(b_j^k - a_j^k)\}$.

4.1.3 BINNING APPROACH

Structured feature vectors can be constructed by simple yet effective approach of binning. The idea is to discretize the filtration domain into various same size bins (see Figure 5). For PBs, one dimensional bins are used, i.e., $[x_i, x_{i+1}]$, $i = 0, 1, \dots, n$ with $x_0 = 0$ and $x_n = r_f$ (with r_f the filtration ending value).

1. For persistent Betti number and persistent Betti function, the binning process can be done easily by collecting their values at the grid points (Cang and Wei, 2017c; Cang et al., 2018), that is, the set $\{f(x_i, L_k) | i = 0, 1, \dots, n; k = 0, 1, 2\}$. In this way, we can systematically obtain n features for each Betti number.
2. For persistent landscapes $\lambda_m(x)$, the same binning process as stated above can be done repeatedly for m times. The m set of $\{\lambda_m(x_i) | i = 0, 1, \dots, n\}$ values are used as features (Bubenik and Dłotko, 2017).
3. For persistent image (Adams et al., 2017), the binning process is based on the rotated PD. Essentially, the computational domain of the rotated PD can be discretized in $n \cdot n$ grids (or pixels) and persistent image values can be evaluated on each grid. Therefore, there are totally $n \cdot n$ features in persistent image vector.
4. The distribution functions of BTs, DTs and PLs can be discretized and used as feature vectors (Cang and Wei, 2017c; Cang et al., 2018). The idea is very straightforward. For each interval $[x_i, x_{i+1}]$, we can count the numbers of the k -th dimensional BTs, DTs, PLs located in this range, and denoted them as $N_{BT}^{k,i}, N_{DT}^{k,i}, N_{PL}^{k,i}$, respectively. The sets of count numbers $\{N_{BT}^{k,i}, N_{DT}^{k,i}, N_{PL}^{k,i} | i = 0, 1, \dots, n; k = 0, 1, 2\}$ can be assembled as a feature vector. It should be noticed that normally for Betti-0, the BTs are 0, thus DTs are usually equal to PLs. So only the set of $\{N_{PL}^{0,i} | i = 0, 1, \dots, n\}$ is used.

5. Similarly, if we consider the PD representation (Cang and Wei, 2017c; Cang et al., 2018), we can discretize the diagram domain into a mesh and count the number of points in each grid. We can also consider the rotated PD and count the point numbers in each grid. These numbers form a same-size vector and can be used as the feature vector.

4.1.4 PERSISTENT CODEBOOK

Instead of using the regular mesh, persistent codebooks are proposed by using different clustering or bagging of the PD points (Zielinski et al., 2018; Bonis et al., 2016).

1. The idea of persistent bag of words (P-BoW) is to assign the points in the rotated PD $T(L_k) = \{T(\vec{l}_j^k) = (a_j^k, b_j^k - a_j^k)\}$ to a precomputed codebook. In P-BoW, the K-means clustering algorithm is employed to cluster the points $T(L_k)$ into n clusters, i.e., $NN(T(\vec{l}_{i,m}^k)) = i (i = 1, 2, \dots, n; m = 1, 2, \dots, N_i)$. Here $NN(x, y) = i$ means point (x, y) belongs to cluster i and N_i is the total number of points in i -th cluster. Further we denote $\vec{x}_i = (x_i, y_i)$ as the cluster center and the P-BoW representation is $\vec{v} = (v_i = |\vec{x}_i|)_{i=1,2,\dots,n}$. To further consider the persistence information, the weight function $w(x, y, t_1, t_2)$ as in persistent surface is considered. Usually, the parameters t_1 and t_2 are set to the persistence values corresponding to 0.05 quantile of birth time and 0.95 quantile of death time, respectively. The weighted K-means clustering provides a more adaptive codebook.
2. Persistent vector of locally aggregated descriptors (P-VLAD) uses the K-means clustering as in P-BoW and then the accumulated distance between a point $T(\vec{l}_{i,j}^k)$ to the nearest codeword \vec{x}_i is computed as following $\vec{v}_i = \sum_{m=1,2,\dots,N_i} (T(\vec{l}_{i,m}^k) - \vec{x}_i)$ with N_i the total number of points in i -th cluster. These n vectors can be concatenated into a $2n$ dimensional vector. It can capture more information than the P-BoW.
3. Persistent Fisher vector (PFV) is to characterize the rotated PD with a gradient vector from a probability model. We let $\lambda_{\text{GMM}} = \{w_i, \vec{\mu}_i, \sum_i; i = 1, 2, \dots, m\}$ be the set of parameters of Gaussian mixture models (GMMs), where w_i , μ_i and \sum_i denote the weight, Gaussian center and covariance matrix of i -th Gaussian, respectively. The likelihood that point $T(\vec{l}_j^k)$ is generated by i -th Gaussian is denoted as $p_i(T(\vec{l}_j^k)|\lambda_{\text{GMM}})$,

$$p_i(T(\vec{l}_j^k)|\lambda_{\text{GMM}}) = \frac{\exp\{-\frac{1}{2}(T(\vec{l}_j^k) - \vec{\mu}_i)' \sum_i^{-1} (T(\vec{l}_j^k) - \vec{\mu}_i)\}}{2\pi |\sum_i|^{\frac{1}{2}}}$$

and the function is

$$\mathcal{F}(T(L_k)|\lambda_{\text{GMM}}) = \sum_j \log\left(\sum_i w_i p_i(T(\vec{l}_j^k)|\lambda_{\text{GMM}})\right).$$

When the covariance matrices are diagonalized, the derivations $\frac{\partial \mathcal{F}(T(L_k)|\lambda_{\text{GMM}})}{\partial \mu_i}$ and $\frac{\partial \mathcal{F}(T(L_k)|\lambda_{\text{GMM}})}{\partial \sigma_i}$ can be evaluated. Here the σ_i is the diagonal element of \sum_i . The PFV is the concatenation of these partial derivatives.

4.1.5 PERSISTENT PATHS AND SIGNATURE FEATURES

Recently, a new feature map for barcodes is proposed (Chevyrev et al., 2018). This model includes two major steps. First, to embed the barcode information into persistent path. Several embeddings are proposed, including landscapes embedding, envelope embedding, Betti embedding and Euler embedding. The persistent landscapes $\lambda_m(x)$ is a typical example of embedding barcodes into path information. Second, from persistent path to tensor series. And tensor series can be used as feature vectors.

4.1.6 2D/3D REPRESENTATION

Two or three dimensional matrixes can be generated from PD, multi-dimensional PH and element-specific PH (Cang and Wei, 2017c; Cang et al., 2018). The persistent surface is an example of 2D

representation. In multi-dimensional PH, we stack each persistent Betti number along the other filtration parameter, this results in a 2D image. If three filtration parameters are considered, a 3D matrix will be generated. Similarly, in element-specific PH, each type of atom combination will contribute seven distributions for BTs, DTs and PLs, all types atoms together form 7 matrixes. Unlike the feature vector representations, these matrix representation can be treated as images and combined directly with convolution neural network (CNN).

4.1.7 NETWORK LAYER FOR TOPOLOGICAL SIGNATURE

A parameterized network layer for topological signatures is proposed in (Hofer et al., 2017). We denote $R^+ = (0, \infty)$ and $R_0^+ = [0, \infty)$. We let $\vec{\mu} = (\mu_0, \mu_1)^T \in R \times R_0^+$ and $\vec{\sigma} = (\sigma_0, \sigma_1) \in R^+ \times R^+$ and $v \in R^+$. We can define,

$$s(l_j^k, \vec{\mu}, \vec{\sigma}, v) = \begin{cases} e^{-\sigma_0^2(a_j^k - \mu_0)^2 - \sigma_1^2(b_j^k - \mu_1)^2}, & b_j^k \in [v, \infty); \\ e^{-\sigma_0^2(a_j^k - \mu_0)^2 - \sigma_1^2(\ln(\frac{b_j^k}{v}) + v - \mu_1)^2}, & b_j^k \in (0, v); \\ 0, & b_j^k = 0. \end{cases}$$

and $S(\vec{\mu}, \vec{\sigma}, v) = \sum_j s(l_j^k, \vec{\mu}, \vec{\sigma}, v)$. For a set of N different parameter pairs $(\vec{\mu}_i, \vec{\sigma}_i), i = 1, 2, \dots, N$, we can concatenate all the corresponding function values together as a vector $(S(\vec{\mu}_i, \vec{\sigma}_i, v))_{i=1,2,\dots,N}$. This vector is then the output of the network layer.

4.2 Persistent-Homology-based Kernel Methods

With the significant role of kernels in machine learning models, one can propose suitable kernel functions for the topological data to replace the role of features. Since similarity measures can be modified into kernels (Chen et al., 2009), we are keen to develop similarity measurement for PH. Moreover, some kernels are separately proposed from the topological perspectives.

4.2.1 SIMILARITY MEASUREMENT

The unique format of PH outcomes poses a great challenge for a meaningful metrics. To solve this problem, distance measurements or metrics (Mileyko et al., 2011; Turner et al., 2014; Chazal et al., 2017; Carriere and Bauer, 2018; Anirudh et al., 2016b) have been considered, including Gromov-Hausdorff distance, Wasserstein distance (Mileyko et al., 2011), bottleneck distance (Mileyko et al., 2011), probability-measure-based distance (Chazal et al., 2011; Marchese and Maroulas, 2017; Chazal et al., 2017), Fisher information metric (Anirudh et al., 2016b).

Definition 32 *The bottleneck distance between two sets of barcodes L_k and L'_k is defined as*

$$d_B(L_k, L'_k) = \inf_{\gamma} \sup_j \|l_j^k - \gamma(l_j^k)\|_{\infty},$$

here γ ranges over all bijections from barcodes L_k to barcodes L'_k . The distance between two barcodes $L_{k,j}$ and $L'_{k,j}$ is defined as $\|l_j^k - l_{j'}^k\|_{\infty} = \max\{|a_{k,j} - a_{k,j'}|, |b_{k,j} - b_{k,j'}|\}$.

Definition 33 *The p -Wasserstein distance between two barcodes is defined as follows,*

$$d_{W,p}(L_k, L'_k) = \inf_{\gamma} \left[\sum_j \|l_j^k - \gamma(l_j^k)\|_{\infty}^p \right]^{\frac{1}{p}}.$$

Again γ is bijection from barcodes L_k to barcodes L'_k . Parameter p is a positive integer.

Definition 34 The Sliced Wasserstein (SW) distance between two barcodes is defined as follows. For a $\theta \in [-\pi/2, \pi/2]$, we can define a line $f(\theta) = \{\lambda(\cos \theta, \sin \theta) | \lambda \in \mathbb{R}\}$. Further $\pi_\theta : \mathbb{R}^2 \rightarrow f(\theta)$ is defined as the orthogonal projection of a point onto this line and the π_Δ is the orthogonal projection onto the diagonal line (i.e., $\theta = \pi/4$). If we denote $\mu(\theta, L_k) = \sum_j \delta_{\pi_\theta(l_j^k)}$ and $\mu_\Delta(\theta, L_k) = \sum_j \delta_{\pi_\theta \circ \pi_\Delta(l_j^k)}$, the SW distance is defined as,

$$SW(L_k, L'_k) = \frac{1}{2\pi} \int \mathcal{W}(\mu(\theta, L_k) + \mu_\Delta(\theta, L'_k), \mu(\theta, L'_k) + \mu_\Delta(\theta, L_k)) d\theta,$$

where the function $\mathcal{W}(x, y)$ is the generic Kantorovich formulation of optimal transport.

4.2.2 TOPOLOGICAL KERNEL

From the topological perspectives, various PH-based kernels have also been proposed, which are listed as follows.

Definition 35 Persistent scale space kernel (PSSK) is proposed by (Reininghaus et al., 2015) as follows.

$$\kappa_{\text{PSSK}}(L_k, L'_k, \sigma) = \frac{1}{8\pi\sigma} \sum_{l_j^k \in L_k, \overline{l_j^k} \in L'_k} e^{-\frac{\|l_j^k - \overline{l_j^k}\|^2}{8\sigma}} - e^{-\frac{\|\overline{l_j^k} - l_j^k\|^2}{8\sigma}},$$

where $\overline{l_j^k}$ is l_j^k mirrored at the diagonal.

Definition 36 Universal persistence scale-space kernel (u-PSSK) is proposed by (Kwitt et al., 2015) as follows.

$$\kappa_{\text{uPSSK}}(L_k, L'_k, \sigma) = e^{\kappa_{\text{PSSK}}(L_k, L'_k, \sigma)}$$

Definition 37 Persistent weighted Gaussian kernel (PWGK) is proposed by (Kusano et al., 2016) as follows.

$$\kappa_{\text{PWGK}}(L_k, L'_k, \sigma) = \sum_{l_j^k \in L_k, \overline{l_j^k} \in L'_k} w_{\text{arc}}(l_j^k) w_{\text{arc}}(\overline{l_j^k}) e^{-\frac{\|l_j^k - \overline{l_j^k}\|^2}{2\sigma^2}}$$

here $w_{\text{arc}}(l_j^k) = \arctan(C(b_j^k - a_j^k)^p)$ with parameter C and p all positive value.

Definition 38 Geodesic topological kernel (GTK) is proposed by (Padellini and Brutti, 2017) as follows.

$$\kappa_{\text{GTK}}(L_k, L'_k, \sigma) = e^{\left\{\frac{1}{h} d_{W,2}(L_k, L'_k)\right\}^2}$$

with $h > 0$ and $d_{W,2}(L_k, L'_k)$ the 2-Wasserstein distance. Similarly, the geodesic Laplacian kernel (GLK) is defined as

$$\kappa_{\text{GLK}}(L_k, L'_k, \sigma) = e^{\left\{\frac{1}{h} d_{W,2}(L_k, L'_k)\right\}}$$

Definition 39 Persistence Fisher Kernel is proposed by (Le and Yamada, 2018) as follows. We let

$$\rho(x, y, L_k) = \frac{1}{Z} \sum_j^{N_k} N(x, y | l_j^k, \sigma).$$

with $Z = \int \sum_j^{N_k} N(x, y | l_j^k, \sigma) dx dy$ and $N(x, y | l_j^k, \sigma) = \frac{1}{\sqrt{2\pi\sigma^2}} e^{-\frac{(x-a_j^k)^2 + (y-b_j^k)^2}{2\sigma^2}}$ is the normal distribution. Further we define the Fisher information metric (FIM) between L_k and L'_k as

$$d_{\text{FIM}}(\rho(x, y, L_k), \rho(x, y, L'_k)) = \arccos \left(\int \sqrt{\rho(x, y, L_k \cup \pi_\Delta(L'_k)) \rho(x, y, L'_k \cup \pi_\Delta(L_k))} dx dy \right)$$

The persistent Fisher kernel (PFK) is defined as,

$$\kappa_{\text{PFK}}(L_k, L'_k) = e^{-t_0 d_{\text{FIM}}(\rho(x,y,L_k), \rho(x,y,L'_k))}.$$

Parameter t_0 is a positive scale value. The PFK is positive definite.

Definition 40 Three persistent-landscape-based kernels are defined as follows.

1. *Global PH kernel (GPHK):* For two persistent landscape functions $\lambda_m(x)$ and $\lambda'_m(x)$, the GPHK is defined as

$$\kappa_{\text{GPHK}}(\lambda_m, \lambda'_m) = \langle \lambda_m, \lambda'_m \rangle = \int \lambda_m(x) \lambda'_m(x) dx.$$

2. *Multiresolution PH kernel (MPHK):* Let $B(c,r)$ be the ball center at point c with radius r . We define a local homology by only considering the points within the ball $B(c,r)$ and filtration process is only performed for these special points. Local persistent landscape functions $\lambda_B(c,r)$ can be derived. If we choose the ball centers from a uniform distribution (\mathcal{P}_C) over the whole point cloud data X , the expected persistent landscape is obtained by $\pi_r = \mathbb{E}_{c \in \mathcal{P}_C} \lambda_{B(c,r)}$. To obtain topological information of X at finer resolutions, we consider M decreasing radius $r_1 > r_2 > \dots > r_M$, and compute the corresponding expected persistent functions $\pi_{r_1}, \pi_{r_2}, \dots, \pi_{r_M}$. We can define the MPMK as

$$\kappa_{\text{MPHK}} = \sum_i^M w_i \langle \pi_{r_i}, \pi'_{r_i} \rangle,$$

where the parameters w_i are nonnegative weights to combine different resolutions. For instance, they can be chosen as $w_i = (r_1/r_i)^3$.

3. *Stochastic multiresolution PH kernel (SMURPHK):* It aims to reduce the computational cost of the MPMK above. Essentially, $\pi_r = \mathbb{E}_{c \in \mathcal{P}_C} \lambda_{B(c,r)}$ can be approximated by considering n centers in the probability function \mathcal{P}_C and s bootstrap samples in $\lambda_{B(c,r)}$. In this way, an average persistent landscape function can be defined as $\bar{\lambda}_r = \frac{1}{ns} \sum_{i=1}^n \sum_{j=1}^s \lambda_{b_j}(c,r)$. Then the SMURPHK is defined as

$$\kappa_{\text{SMURPHK}} = \sum_i^M w_i \langle \bar{\lambda}_{r_i}, \bar{\lambda}'_{r_i} \rangle.$$

4.3 Machine Learning Algorithms

4.3.1 SUPPORT VECTOR MACHINE (SVM)

Support vector machines (SVM), proposed in (Cortes and Vapnik, 1995), is a supervised learning algorithm that finds the optimal hyperplane/decision boundary of the form $\mathbf{w}^T \mathbf{x} + b = 0$ in the context of 2-class classification problems. This creates a quadratic optimisation problem to solve for coefficients \mathbf{w} and b . The primal problem is formulated as:

$$\min_{\mathbf{w}, b} \frac{1}{2} |\mathbf{w}|^2 + C \sum \xi(\mathbf{w}; \mathbf{x}_i, y_i),$$

where $\xi(\mathbf{w}; \mathbf{x}_i, y_i)$ is a convex non-negative loss function. The above L2-regularised classifier can also be modified into an L1-regularised classifier together with different loss function used. Rewriting the problem to involve Lagrange multipliers converts the primal problem that optimises (minimises) with respect to coefficients \mathbf{w} into the dual problem that optimises (maximises) with respect to the multipliers. Detailed derivation of the optimal hyperplane algorithms and soft margin classifiers can be found in (Cortes and Vapnik, 1995). The method is popular for its robustness to individual

observations, compared to discriminant analysis (with the use of support vectors, namely only the training observations that lie within the margins are used).

In some cases, however, if the data is linearly inseparable, it requires the use of feature expansion, i.e. to map the data into a higher dimensional space $\Psi : \mathbb{R}^{\mathcal{N}} \rightarrow \mathbb{R}^{\mathcal{M}}, \mathcal{N} < \mathcal{M}$. Such a transformation involves the use of kernel functions. The kernels proposed in Section 4.2 can play an important role here. Alternatively, one can consider the kernels based on structured features, such as the Gaussian kernel $K(\mathbf{x}_i, \mathbf{x}_j) = \exp(-\gamma|\mathbf{x}_i - \mathbf{x}_j|^2), \gamma > 0$, where the feature space is implicit and high dimensional. The classifier formed is the radial basis function (**RBF**) **SVM**, where the separating hyperplane involving $f(\mathbf{x}) = \sum_{i=1}^N \alpha_i y_i \exp(-\gamma|\mathbf{x} - \mathbf{x}_i|^2) + b$. Here, γ is used as a tuning parameter to determine the smoothness of the decision boundary formed. A large value of γ used corresponds to a more complex boundary formed that is more prone to overfitting and vice versa. Depending on the complexity and the nature of the classification problem, different kernels or classifier types may be found to be more suitable.

There are various available software packages that support various types of (regularised) SVM. In our study, the R packages used are **Liblinear** and **e1071**.

The **Liblinear** package is particularly useful and efficient for large data sets (especially with many features). In subsequent experiments, only the following three types of support vector classifiers (SVCs) using primal solvers will be used as the equivalence between primal and dual solvers was shown in (Fan et al., 2008).

1. The L2-regularised logistic regression (**Liblinear-s0**) that solves

$$\min_{\mathbf{w}} \frac{1}{2} \mathbf{w}^T \mathbf{w} + C \sum_{i=1}^l \log(1 + e^{-y_i \mathbf{w}^T \mathbf{x}_i});$$

2. The L2-regularised L2-loss SVC (**Liblinear-s2**) that solves

$$\min_{\mathbf{w}} \frac{1}{2} \mathbf{w}^T \mathbf{w} + C \sum_{i=1}^l (\max(0, 1 - y_i \mathbf{w}^T \mathbf{x}_i))^2;$$

3. The L1-regularised L2-loss SVC (**Liblinear-s5**) that solves

$$\min_{\mathbf{w}} |\mathbf{w}|_1 + C \sum_{i=1}^l (\max(0, 1 - y_i \mathbf{w}^T \mathbf{x}_i))^2,$$

where $|\cdot|_1$ is the L1-norm. This type of regularised classifier creates sparse solutions with selection of nonzero features.

For these solvers, the one-vs.-rest approach will be used for multi-class classification. The tuning parameter C in the formulations above helps to weigh between the regularisation of the weights used (solution for \mathbf{w}) and the loss function. The former is favoured when C is small or when the number of observations is much less than the number of features (high-dimensional data).

4.3.2 TREE-BASED METHODS

A decision tree is a process of searching through then dividing the predictor space (set of possible values for each feature x_1, x_2, \dots, x_p into distinct, non-overlapping regions). The structure of a classification tree is that splits are made at one of the p predictors and terminates at nodes with the output class predictions for the region. The same prediction will be made for every observation that lies in the same region. The tree is grown by recursive binary splitting with the aim of minimising resultant misclassification error, Gini index, or cross-entropy.

This simple algorithm, that splits the original predictor space into rectangles, is widely known to have easy interpretation but suffers from low accuracy when it begins to overfit the data. The size of the tree is the main tuning parameter, where a large tree performs well in the training set but risks “overfitting” the data (resulting in high variance, low bias) while a smaller tree involves lower variance but higher bias. Possible strategies include growing the tree to a large size before pruning it into a smaller tree with cross validation (**Pruned tree**, see (Breiman et al., 1984)) or using bagging approach to reduce variance from multiple (uncorrelated) decision trees (**Random forest**, see (Breiman, 2001)) or using boosting to sequentially improve the previous models by adding weak learners to correct classification errors (**Boosted trees**, see (Freund and Schapire, 1997; Friedman, 2001)).

Key advantages of tree-based methods is that data pre-processing is not required as inputs are directly used to generate the decision trees. Large amounts of input features can be used without modification or scaling with an inherent “feature selection” process by selecting order of splits according to variable importance. The most important predictors are first chosen for the initial splits in the tree while unimportant features can be left unused. This is particularly advantageous in our context as it is able to help us interpret the uses of the binned features and identify the events (birth, death or persistence) that are critical for good predictions. The variable importance measures allow us to see which are the important predictors.

4.3.3 NEURAL NETWORKS WITH DROPOUT

Neural Networks (NNs) are a popular choice of mathematical modelling inspired by biological neural networks. It works on the basis of transforming the linear combinations of original input features through the use of activation functions and has the effect of creating highly non-linear classifiers. As such, the method is known for its high accuracy and predictive abilities, which often surpasses robust methods like SVM. The complexity of the model depends on the number of hidden layers and the number of units in each layer. Information is passed down from the input layer to the hidden layers to the final output layer through the use of activation functions and linear combinations of weights on units. The output function for binary classification is the sigmoid function while that for multi-class classification is the softmax function.

Many extensions of NNs such as convolution neural networks (CNNs) have been employed for topological data, including the recent paper (Cang and Wei, 2017c), which uses multi-task multi-channel topological convolutional neural networks to learn from small and noisy training data. Deep NNs involve the embedding of multiple non-linear hidden layers that allows them to model complex relationships between features and output. However, the highly non-linear classifier trained may suffer from the effects of overfitting the training data, resulting in poor out-of-sample test performance. As such, regularisation methods, especially dropout (Srivastava et al., 2014), have been introduced to address the overfitting problem. This concept has been widely applied and cited to have obtained surprisingly excellent results with significant improvement to existing standard neural networks.

The key features in the use of dropout is that units are randomly dropped along with their incoming and outgoing connections from the network. Each unit is dropped out randomly and independently of other units. Let p to be the probability of a unit being dropped. The dropped out unit is then temporarily excluded from the network and their corresponding weights will not be updated in that iteration. The method of obtaining weights is still unchanged in a basic feed-forward neural networks setting (through backward propagation and convergence to obtain best weights with lowest cost). The resulting thinned neural network can then achieve the effect of preventing complex co-adaptation in the training of the weights compared to a fully connected neural network by adding noise to the hidden units. At test time, the network is all fully connected and the trained weights are then multiplied with a probability of $1 - p$. For more details about the dropout, we refer the readers to (Srivastava et al., 2014).

5. Protein Secondary Structure Classification using PHML

5.1 The Classification Problem

Our classification problem uses the dataset downloaded from the Structural Classification of Proteins-extended (SCOPe) database (Fox et al., 2014), from which we randomly sample 450 protein samples for our classification task. More details into how the database is structured and various classification tasks can be found in (Murzin et al., 1995).

Each protein sample is labeled as one of three classes, namely 1) all-alpha helix, 2) all-beta pleated sheets, and 3) mixed alpha-beta domains, where the alpha (α)-helix and the beta (β)-pleated sheets are two main types of protein secondary structure and their properties are documented in Appendix A. For illustrative purpose, we consider a balanced class problem with an equal number of 150 protein samples from each of the three class. Out of 150 samples in each class, 120 of them are used for training while the remaining 30 are used for testing. Our objective is to classify each test sample into one of these three classes based on its structure information. We consider the coarse-grained (CG) representation, i.e., one alpha-carbon (C_α) for each residue (Xia and Wei, 2014). As in the first two steps of the general pipeline for PHML, protein structures will be represented by either the Rips complex (RC) or the Alpha complex (AC).

5.1.1 PROCEDURE AND EVALUATION METHODOLOGY

We conduct our studies with the following steps:

Step 1 Obtain RC or AC barcodes (Dim-0, 1, 2) for each of the protein samples (see Section 3.1).

Step 2 Generate three sets (Dim-0, 1, 2) of barcodes with the obtained complexes (see Section 3.2).

Step 3 Extract topological feature representation (TFR) from each set of barcodes for each protein sample to obtain an overall data matrix with n observations and p features (see Section 4.1). In this study, we consider two TFRs: 1) barcode statistics (BS) and 2) binned features (BF).

Step 4 Train the model using the data matrix of the training dataset (see Section 4.3) and evaluate the trained classifier with the test dataset.

In Step 3, for the TFR of BF, the bin size used was fixed at 0.5\AA for both the RC and AC filtrations. Moreover, the maximum filtration distance L was set to be $L = 20\text{\AA}$ for RC filtration and $L = 50\text{\AA}$ for AC filtration. Notice that there are three dimensions for the protein’s structure. Hence, the training data matrix has $n = 360$ rows/observations and the number of its columns/features p is equal to 13 (for BS with RC or AC), 360 (for BF with RC), or 900 (for BF with AC).

In Step 4, the common metric for evaluating the performance of models is the overall accuracy of the predictions for the 90 held-out test samples. However, one can also cross-tabulate the output class predictions with the true classes to evaluate class-specific prediction accuracy. While the use of accuracy measure is commonly used to evaluate the performance of balanced-class classifiers, it is unable to distinguish between the severity of the errors. For example, in the context of our classification problem, the failure to distinguish between class 2 (all-alpha) and class 3 (all-beta) should be considered more severe than errors involving class 1 (mixed alpha and beta). Therefore, one can further distinguish the types of misclassifications into 2 categories:

Type-I Error Misclassification errors rate involving class 1 (between classes 1 and 2 and between classes 1 and 3);

Type-II Error Misclassification errors rate between classes 2 and 3.

We expect our classifiers to have zero or extremely low second-type error and an acceptable first-type error. For each machine learning model, the output tables generally admit the following format:

- 6 Rows: The evaluation criteria to be compared: three individual accuracies of the classes, two types of errors defined above, and the overall accuracy, respectively.
- 4 Columns: Corresponding results for the combinations of the types of complex used (RC or AC) and the TFRs used (BS or BF).

5.2 Results

5.2.1 RESULTS USING SUPPORT VECTOR MACHINE

Besides of the three types of SVCs in Section 4.3.1, we also add the RBF SVM into the comparison. We rely on R packages `e1071` and `LiblineaR` to implement these four classifiers. Hyperparameters were searched from a grid of $C : 2^{-14}, 2^{-13}, \dots, 2^{14}$ while $g : 2^{-6}, 2^3$ (only for kernels). Cross-validation was performed using the built-in functions in the packages to select optimal parameters (C and γ for RBF SVM classifiers, C for linear SVCs). The above procedure was referenced from that recommended in (Chang and Lin, 2011).

Table 1: Results using SVM with different simplicial complexes and TFR methods.

| Accuracy/ Results | RBF SVM | | | | LiblineaR-s0 | | | |
|----------------------|--------------|-------|--------|-------|--------------|-------|-------|-------|
| | RC-BS | RC-BF | AC-BS | AC-BF | RC-BS | RC-BF | AC-BS | AC-BF |
| Mixed Alpha-Beta | 83.3 % | 73.3% | 80.0 % | 73.3% | 70.0% | 66.7% | 43.3% | 60.0% |
| All Alpha | 86.7 % | 93.3% | 86.7 % | 93.3% | 73.3% | 93.3% | 93.3% | 96.7% |
| All Beta | 86.7 % | 73.3% | 90.7 % | 83.3% | 86.7% | 100% | 96.7% | 100% |
| Type-I Error | 13/90 | 18/90 | 13/90 | 15/90 | 18/90 | 12/90 | 19/90 | 13/90 |
| Type-II Error | 0/90 | 0/90 | 0/90 | 0/90 | 0/90 | 0/90 | 1/90 | 0/90 |
| Overall | 85.6 % | 80.0% | 85.6 % | 83.3% | 80.0% | 86.7% | 77.8% | 85.6% |
| Accuracy/ Results | LiblineaR-s2 | | | | LiblineaR-s5 | | | |
| | RC-BS | RC-BF | AC-BS | AC-BF | RC-BS | RC-BF | AC-BS | AC-BF |
| Mixed Alpha-Beta | 66.7% | 66.7% | 23.3% | 56.7% | 66.7% | 56.7% | 26.7% | 63.3% |
| All Alpha | 83.3% | 93.3% | 96.7% | 96.7% | 83.3% | 93.3% | 26.7% | 96.7% |
| All Beta | 86.7% | 96.7% | 100% | 96.7% | 86.7% | 76.7% | 96.7% | 100% |
| Type-I Error | 19/90 | 12/90 | 24/90 | 14/90 | 19/90 | 22/90 | 23/90 | 12/90 |
| Type-II Error | 0/90 | 1/90 | 1/90 | 0/90 | 0/90 | 0/90 | 1/90 | 0/90 |
| Overall | 78.9% | 85.6% | 72.2% | 84.4% | 78.9% | 75.5% | 73.3% | 86.7% |

Table 1 presents the results for the protein structure classification using SVM. From the results, we can observe that if we adopt BS for TFR, **RBF SVM** uniformly outperform other SVCs, implying that the data represented by BS are not linearly separable and transformation with Gaussian kernel is helpful; if we adopt BF for TFR, the SVCs generally outperform **RBF SVM** and among them, L2-regularised logistic regression (**LiblineaR-s0**) and L2-regularised L2-loss SVC (**LiblineaR-s2**) perform similarly while L1-regularised L2-loss SVC (**LiblineaR-s5**) performs the best when we consider AC and BF. The Type-II error occurs only when we consider **LiblineaR-s2** with RC and BF and when AC and BS are used, whom we do not recommend. We postulate that among all

combinations of the types of complex used and the TFRs used, AC and BF carry the most structure information; however, they brought the challenge of high-dimensional statistics as $n \approx p$. SVCs with regularizations can remedy the overfitting issue and give a decent classification result.

5.2.2 RESULTS USING TREE-BASED METHODS

A baseline of comparison across tree-based methods was set using a single **Pruned tree** implemented using the R package **tree**. A 10-fold (default value) cross-validation was performed to search for the optimal size of tree. **Random forest** was implemented with $mtry = \sqrt{p}$ (number of features randomly sampled as candidates at each split) and $n_{trees} = 1000$ (number of bootstrapped trees to grow) using the R package **randomForest**. **Boosted trees** were implemented using R package **adaBag** with a detailed accompanying tutorial (Alfaro et al., 2013). The boosted trees used are the stumps (with $maxdepth=1$) and a fixed maximum number of iterations/trees (e.g. 100, 200) were used before searching for the optimal number of iterations that prevents overfitting of the errors. The optimal number of iterations is found by taking value that corresponds to lowest test error. Signs of overfitting are observed when the test error starts to increase after a certain number of iteration and the ensemble can be pruned as well using the built-in function. The package is also suitable for multi-class classification problems where AdaBoost-SAMME (Hastie et al., 2009) is adopted.

Table 2: Results using tree-based methods with different simplicial complexes and TFR methods. *Tuned parameter refers to the size of pruned tree or the number of iterations in the boosting approach.

| Accuracy/ Results | Pruned tree | | | | Boosted trees | | | |
|----------------------|-------------|-------|--------|-------|---------------|-------|-------|-------|
| | RC-BS | RC-BF | AC-BS | AC-BF | RC-BS | RC-BF | AC-BS | AC-BF |
| Mixed Alpha-Beta | 70.0 % | 63.3% | 36.7 % | 76.7% | 76.7% | 80.0% | 66.7% | 96.7% |
| All Alpha | 90.0 % | 93.3% | 86.7 % | 93.3% | 86.7% | 93.3% | 83.3% | 86.7% |
| All Beta | 90.0 % | 86.7% | 80.0 % | 76.7% | 93.3% | 93.3% | 83.3% | 96.7% |
| Type-I Error | 15/90 | 17/90 | 26/90 | 16/90 | 13/90 | 10/90 | 20/90 | 6/90 |
| Type-II Error | 0/90 | 0/90 | 3/90 | 0/90 | 0/90 | 0/90 | 0/90 | 0/90 |
| Overall | 83.3 % | 81.1% | 67.8 % | 82.2% | 85.6% | 88.9% | 77.8% | 93.3% |
| Tuned* parameter | 3 | 9 | 7 | 4 | 9 | 37 | 74 | 81 |

| Accuracy/ Results | Random forest | | | |
|----------------------|---------------|-------|-------|-------|
| | RC-BS | RC-BF | AC-BS | AC-BF |
| Mixed Alpha-Beta | 86.7% | 86.7% | 66.7% | 73.3% |
| All Alpha | 86.7% | 93.3% | 83.3% | 90.0% |
| All Beta | 93.3% | 86.7% | 83.3% | 96.7% |
| Type-I Error | 10/90 | 10/90 | 20/90 | 12/90 |
| Type-II Error | 0/90 | 0/90 | 0/90 | 0/90 |
| Overall | 88.9% | 88.9% | 77.8% | 86.7% |

Table 2 reports the results using tree-based methods. Except for **Pruned tree** with AC and BS, there were no misclassifications between class 2 and 3 (Type-II error). Using AC and BS still yield the worst results as with SVM methods. No matter what complex or TFR are used, bagging (**Random**

forest) and boosting (**Boosted trees**) can significantly improve the out-of-sample performance. Again, the best result can be found at using AC and BF together with **Boosted trees** and the best accuracy could hit 93.3%.

With the careful selection of appropriate tuning parameters such as the number of splits/depth and the number of iterations, modified tree-based models can prevent over-fitted errors or generalize well by converting multiple weak learners into a strong learner. Moreover, tree-based methods possess the advantage of dealing with many correlated input features as there is an inherent “variable selection” process when searching through all variables for the best split. Using variable importance measures, one can also infer the key barcodes to distinction. Aggregating the top 5 variable importance results from all boosting and random forest models, we notice that none of them are binned features involving Dim-0 as expected and the important variables are consistently identified from the same binned barcodes except for its order of importance.

5.2.3 RESULTS USING NEURAL NETWORKS

The results for types of neural networks are reported: 1) the simplest one-hidden-layer NN; 2) a multiple-layer NN with dropout. For the first type of NN, we simply apply R package `nnet` but we repeated the training 30 times to obtain the best weights with the lowest cost to avoid a solution from converging to a local minimum. We call it **Repeated Net**. For the second type of NN, the dropout network was implemented using the R package `keras`.

In our application, the number of training parameters is often much greater than the number of the available samples for the use of (deep) NNs, which possibly result in overfitting. The data pre-processing, involved removal of constant variables with near-zero variance and subsequent normalisation, is required for the implementation. Preliminary tests without such pre-processing resulted in poor training of weights as the variables with greater numeric ranges dominate those in smaller numeric ranges. The resulting model has even poor training accuracy whereby the in-sample error is inconclusive as well.

Notice that there is no formula for the number of hidden layers and the number of units in the hidden layer. One can choose to add or remove layers conveniently using the `keras` package. Cross-validation can be used to tune for the optimal number of units but it also involves a series of trial-and-error and is heavily dependent on the nature of the data as well. In a recent paper (Lin et al., 2017), it concludes that a neural network using p input features should not be fitted with fewer than $U = 2^p$ units in the hidden layer. However, due to limited computational time and power, the number of units in the single hidden layer was set at $U = 2^7$ (resp. 2^4) for all experiments involving **Repeated Net** and BS (resp. BF) input features. Errors involving insufficient memory allocation might be presented when the number of hidden units is too large.

Deep neural networks (**Deep Net**) with or without dropout were applied using the R package `keras`. The network architecture used is “ p (Input)- X - X - $2X$ -3 (Output),” where $X = 128$ refers to the number of units in the first two hidden layers while twice that is used in the last hidden layer. The size of each hidden layer used in the **Deep Net** is modified with reference to that used in (Srivastava et al., 2014). The dropout approach with $p = 0.3$ was performed for all hidden layers. The network with Rectified Linear Units (ReLUs) was trained using stochastic gradient descent with a learning rate of 0.4, a decay rate of 0.01, an epoch size of 450, a batch size of 200, and validation split of 20%.

Table 3 reports the results using NNs. For the **Deep Net**, we do not report the results for using BS to save space, because as with most experiments with the ML algorithms presented so far, using BF is better than using BS. It can be seen that a **Deep Net** is better than a **Repeated Net** and the dropout approach can slightly improve the performance of a **Deep Net**. Moreover, the **Deep Net** provides a relatively high and robust performance with different complexes.

To wrap up the discussions above, we consistently observe that the BF is a better TFR than the BS while different complexes used will slightly affect the performance. When BF is used, it is crucial

Table 3: Results using NN with different simplicial complexes and TFR methods.

| Accuracy/ Results | Repeated Net | | | | Deep Net | | | |
|----------------------|--------------|-------|--------|-------|------------|-------|--------------|-------|
| | | | | | No dropout | | With dropout | |
| | RC-BS | RC-BF | AC-BS | AC-BF | RC-BF | AC-BF | RC-BF | AC-BF |
| Mixed Alpha-Beta | 70.0% | 76.7% | 63.3% | 60.0% | 90.0% | 73.3% | 90.0% | 76.7% |
| All Alpha | 90.0 % | 93.3% | 83.3 % | 100% | 90.0% | 90.0% | 90.0% | 90.0% |
| All Beta | 83.3% | 83.3% | 83.3 % | 93.3% | 90.0% | 100% | 93.3% | 100% |
| Type-I Error | 16/90 | 14/90 | 19/90 | 14/90 | 9/90 | 11/90 | 8/90 | 10/90 |
| Type-II Error | 0/90 | 0/90 | 2/90 | 0/90 | 0/90 | 0/90 | 0/90 | 0/90 |
| Overall | 81.1 % | 84.4% | 76.7 % | 84.4% | 90.0% | 87.8% | 91.1% | 88.9% |

for the proposed ML algorithm to possess the ability to address the overfitting problem, especially when AC is also used. In our application, **Boosted tress** and **Deep Net with dropout** perform the best and the overall accuracy can reach more than 90%.

5.3 Further Discussion

On top of the findings in Section 5.2, we further advance our understandings on PHML by exploring the potential improvements from different aspects. In this section, we focus on the BF input features and investigate whether the bin size of BF will be a significant factor in our application. We also explored the usefulness of principal component analysis (PCA) on relieving the high-dimensional learning problem incurred by BF. However, the answer is negative and thus, to save space, we report the corresponding results in the Appendix B for readers' reference.

5.3.1 EFFECTS OF INCREASING BIN NUMBER FOR BINNED FEATURES

In this section, three different bins sizes are considered: 0.5\AA , 0.25\AA , and 0.01\AA . This corresponds to the number of bins of $N=40$, 80, and 200, respectively, for the RC barcodes and $N=100$, 200, and 500, respectively, for the AC barcodes. For each bin, three features are extracted and concatenated and this process is repeated for each of the three dimensions of complexes. Thus, for a protein sample with N bins, the number of features is $9N$. However, the number of training samples is always 360 in our application.

Ideally, the use of more bins may help to represent the protein sample better by identifying more distinguishing features of the barcode (similar to the concept of resolution). However, we do note that the use of too many bins may result in redundant features when the information represented in adjacent bins are the same. The comparison study in this section is to examine the effects of increasing the bin number on the performance of PHML. We remark that in most cases, due to our relatively small sample size, the number of features exceeds the number of samples ($p > n$), which poses high-dimensional learning challenge.

We repeat the experiments in Section 5.2 with different bin numbers. The results are reported in Tables 6-9 which are placed in Appendix C for better layout.

From Table 6, we can observe that increasing the bin numbers does not provide improvement for the SVM approaches and it even causes the RBF SVM to become worse. From the statistical perspective, the linear SVCs are robust to the number of bins/features and provide stable performance.

It can be seen from Table 7 that increasing the bin number does improve the performance of the tree-based methods. With enough bins, the **Random forest** and the **Boosted trees** can

consistently provide about 90% overall accuracy without any Type-II error. We remark that implied from our experimental results, the number of iterations in **Boosted trees** should be cross-validated.

The results in Table 8 clearly indicate that the improvement of **Repeated Net** by increasing the bin number is significant. For the experiments with **Deep Net**, we also adjust the network architectures to reflect the increasing number of bins. It can be seen from Table 9 that the **Deep Net** with more bins as inputs, a more complex network architecture, and the use of dropout improves the performance. By comparing Tables 8 and 9, the largest improvement of 6.7% increase in overall accuracy was observed for two starred numbers. However, when $N = 200$ for RC or 500 for AC, the **Deep Net** performed unsatisfactorily, which could be attributed to many redundant bins formed and serious overfitting issue occurred.

6. Conclusion

PH-generated barcodes are useful to discover underlying topological features using only finite metric data. Our study provides a gentle walk-through of various methods of Topological Feature Representations (TFR) namely the use of Barcode Statistics (BS) or binned features (BF) before applying them to various machine learning techniques such as SVM, tree-based methods, and NN. The purpose of this paper is to provide guidelines for new users of PH softwares and to provide connections between each stage of analysis. This exposes new users to a complete experience of starting with raw data inputs to the final stage of using machine learning techniques on TFRs. For more advanced users, various stages of analysis can be further improved and fine-tuned depending on their needs and available resources.

Although we only illustrate the PHML on point cloud data, the PHML procedure summarized in this paper could also be applied other datasets including networks or image datasets; see Figure 4. An interesting future research is (extremely) imbalanced class problems that are prevalent in some classification problems. From the computational perspective, the methods can also be scaled up for larger datasets by paralleling some processes.

Acknowledgments

This research is partially supported by Nanyang Technological University Startup Grants M4081840 and M4081842, Data Science and Artificial Intelligence Research Centre@NTU M4082115, and Singapore Ministry of Education Academic Research Fund Tier 1 M401110000.

Appendix A. Properties of the Protein Secondary Structure

This section gives a review of some of the key properties of the secondary structure of proteins. The two main types of protein secondary structure are the alpha (α)-helix and the beta (β)-pleated sheets.

The α -**helix** has the following properties:

1. Bond length between immediate C_α atom is 3.8\AA .
 - This corresponds to the length of typical Betti-0 (Dim-0) bars.
2. Each turn is made up of 3.6 amino acid residues.
 - The formation of Betti-1 (Dim-1) bars can be explained using the slicing technique described in (Xia and Wei, 2014).
 - The alpha-helix structure is stabilised by the presence of hydrogen bonds between the amine hydrogen N-H and carbonyl C=O oxygen.

- Each set of 4 C_α atoms form a one-dimensional loop which contributes to a Betti-1 (Dim-1) bar.
3. Absence of Betti-2 (Dim-2) bars where no cavity is formed since there is insufficient "time" such that the loops are filled up as faces before the cavity can be formed for a single alpha helix.

The β -pleated sheets have the following properties:

1. Bond length/distance between immediate C_α atom in the same strand is also 3.8\AA .
 - This corresponds to the length of typical Betti-0 (Dim-0) bars. The bar terminates once the atoms are connected.
2. Each β -pleated sheet is a stretched out polypeptide chain made up of 3 to 10 amino acid residues.
3. The β -pleated sheets are extended structures that are stabilised by hydrogen bonds between residues in adjacent chains.
4. Each strand must be connected to adjacent strands where the shortest distance between C_α and the nearest neighbour in adjacent strand is 4.1\AA .
5. Adjacent chains run parallel or antiparallel to one another.

Appendix B. Principal Component Analysis on Binned Features

In this appendix, we investigate the effects of principal component analysis (PCA) on PHML for our application in Section 5. We do not involve the tree-based methods with PCA because trees process dimension reduction by their own construction.

There are signs of quite high correlation between adjacent BF as seen in Figure 6. The use of bins unavoidably suffers from the curse of dimensionality, especially when there are limited number of samples n and $n \ll p$, where p is the number of features. To tackle such a situation, PCA can be applied to transform features into a few uncorrelated PCs, which can be viewed as new features in a lower dimensional feature space. The downside of such an approach is that the final PCs do not have a clear interpretation to the original bins.

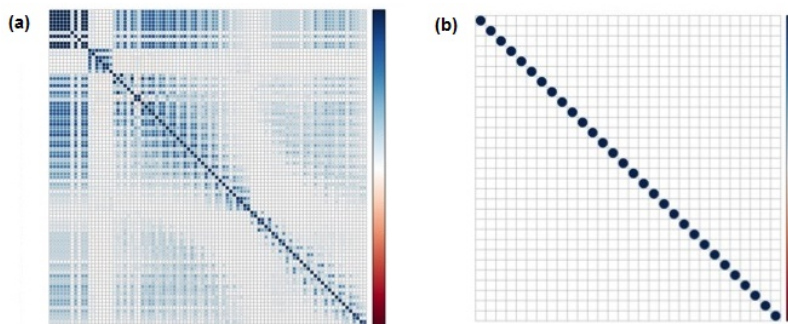


Figure 6: (a) Correlation matrix for the BFs from RC barcodes with 40 bins (where the near-zero variance variables removed). (b) Correlation matrix for the 30 PCs transformed from the same BFs. The blue regions corresponds to high positive correlation and is observed between multiple BFs, in contrast with that in the PCs, where white regions correspond to zero correlation.

In subsequent reports, the experimental results involving principal components transformed from BFs are denoted by an extension “PC”. For consistency, only the first 30 PCs will be used for all transformed features using either RC or AC barcodes. The same set of PCs are used as input features for SVMs and (deep) NNs (with dropout). The settings are the same as specified in Sections 5.2.1 and 5.2.3. Tables 4 and 5 report the corresponding results.

Table 4: Results using SVM with different simplicial complexes and principal components of BFs.

| Accuracy/ Results | RBF SVM | | LiblineaR-s0 | | LiblineaR-s2 | | LiblineaR-s5 | |
|----------------------|---------|-------|--------------|-------|--------------|-------|--------------|-------|
| | RC-PC | AC-PC | RC-PC | AC-PC | RC-PC | AC-PC | RC-PC | AC-PC |
| Mixed Alpha-Beta | 73.3% | 76.7% | 40.0% | 36.7% | 43.3% | 36.7% | 40.0% | 40.0% |
| All Alpha | 93.3% | 93.3% | 96.7% | 96.7% | 96.7% | 96.7% | 100% | 96.7% |
| All Beta | 73.3% | 76.7% | 93.3% | 96.7% | 93.3% | 96.7% | 86.7% | 96.7% |
| Type-I Error | 18/90 | 16/90 | 20/90 | 21/90 | 19/90 | 21/90 | 22/90 | 20/90 |
| Type-II Error | 0/90 | 0/90 | 1/90 | 0/90 | 1/90 | 0/90 | 0/90 | 0/90 |
| Overall | 90.0% | 73.3% | 90.0% | 76.7% | 90.0% | 76.7% | 75.6% | 77.8% |

Table 5: Results using NN with different simplicial complexes and principal components of BFs.

| Accuracy/ Results | Repeated NN | | Deep Networks with dropout | |
|----------------------|-------------|-------|-------------------------------|-------|
| | RC-PC | AC-PC | RC-PC | AC-PC |
| Mixed Alpha-Beta | 66.7% | 60.0% | 60.0% | 56.7% |
| All Alpha | 93.3% | 96.7% | 93.3% | 93.3% |
| All Beta | 86.7% | 86.7% | 93.3% | 96.7% |
| Type-I Error | 16/90 | 17/90 | 16/90 | 16/90 |
| Type-II Error | 0/90 | 0/90 | 0/90 | 0/90 |
| Overall | 82.2% | 81.1% | 82.2% | 82.2% |

By comparing the results in Tables 1 and 4 and Tables 3 and 5, we can see that the use of PCA on BFs does not improve the performance. It implies that the PCA transformation lost information of BFs. In conclusion, it is not recommended that ML algorithms with BFs are incorporated with PCA. However, it does not prohibit PCA from being a powerful visualization tool for the unstructured topological data.

Appendix C. Effects of Increasing Bin Number for Binned features

In Tables 6-9, the first three or four columns specify the settings of PHML and the remaining columns report the evaluation measurements. The highest overall accuracy number across different bin numbers for a given method is highlighted in red.

Table 6: Results using SVM with different simplicial complexes and BF of different bin numbers.

| Steps 1&2 | Step 3 | Step 4 | $N=40$ (RC) or 100 (AC) | | | $N=80$ (RC) or 200 (AC) | | | $N=200$ (RC) or 500 (AC) | | |
|---------------|------------------|--------------|-------------------------|--------------|---------------|-------------------------|--------------|---------------|--------------------------|--------------|---------------|
| | | | Overall | Type-I Error | Type-II Error | Overall | Type-I Error | Type-II Error | Overall | Type-I Error | Type-II Error |
| Rips complex | BF with $L = 20$ | RBF SVM | 80.0% | 18/90 | 0/90 | 75.6% | 22/90 | 0/90 | 76.7% | 21/90 | 0/90 |
| Rips complex | BF with $L = 20$ | LiblineaR-s0 | 86.7% | 12/90 | 0/90 | 86.7% | 12/90 | 0/90 | 82.2% | 15/90 | 1/90 |
| Rips complex | BF with $L = 20$ | LiblineaR-s2 | 85.6% | 12/90 | 1/90 | 83.3% | 15/90 | 0/90 | 84.4% | 14/90 | 0/90 |
| Rips complex | BF with $L = 20$ | LiblineaR-s5 | 85.6% | 12/90 | 1/90 | 86.7% | 12/90 | 0/90 | 81.1% | 17/90 | 0/90 |
| Alpha complex | BF with $L = 50$ | RBF SVM | 83.3% | 15/90 | 0/90 | 72.2% | 25/90 | 0/90 | 78.9% | 19/90 | 0/90 |
| Alpha complex | BF with $L = 50$ | LiblineaR-s0 | 85.6% | 13/90 | 0/90 | 84.4% | 14/90 | 0/90 | 85.6% | 13/90 | 0/90 |
| Alpha complex | BF with $L = 50$ | LiblineaR-s2 | 84.4% | 14/90 | 0/90 | 82.2% | 16/90 | 0/90 | 82.2% | 16/90 | 0/90 |
| Alpha complex | BF with $L = 50$ | LiblineaR-s5 | 86.7% | 12/90 | 0/90 | 83.3% | 15/90 | 0/90 | 82.2% | 16/90 | 0/90 |

Table 7: Results using tree-based methods with different simplicial complexes and BF of different bin numbers. The three maxtree numbers in last two rows correspond to the cross-validated number of iterations for different bin numbers.

| Steps 1&2 | Step 3 | Step 4 | $N=40$ (RC) or 100 (AC) | | | $N=80$ (RC) or 200 (AC) | | | $N=200$ (RC) or 500 (AC) | | |
|---------------|----------------|--|-------------------------|--------------|---------------|-------------------------|--------------|---------------|--------------------------|--------------|---------------|
| | | | Overall | Type-I Error | Type-II Error | Overall | Type-I Error | Type-II Error | Overall | Type-I Error | Type-II Error |
| Rips complex | BF with $L=20$ | Pruned Tree | 81.1% | 17/90 | 0/90 | 83.3% | 15/90 | 0/90 | 84.4% | 14/90 | 0/90 |
| Alpha complex | BF with $L=50$ | Pruned Tree | 82.2% | 16/90 | 0/90 | 84.4% | 14/90 | 0/90 | 80.0% | 18/90 | 0/90 |
| Rips complex | BF with $L=20$ | Random Forest | 88.9% | 10/90 | 0/90 | 87.8% | 11/90 | 0/90 | 86.7% | 12/90 | 0/90 |
| Alpha complex | BF with $L=50$ | Random Forest | 86.7% | 12/90 | 0/90 | 87.8% | 11/90 | 0/90 | 90.0% | 9/90 | 0/90 |
| Rips complex | BF with $L=20$ | AdaBag maxdepth=1 maxtree=100 | 84.4% | 14/90 | 0/90 | 88.9% | 10/90 | 0/90 | 88.9% | 10/90 | 0/90 |
| Alpha complex | BF with $L=50$ | AdaBag maxdepth=1 maxtree=100 | 84.4% | 14/90 | 0/90 | 85.6% | 13/90 | 0/90 | 88.9% | 10/90 | 0/90 |
| Rips complex | BF with $L=20$ | AdaBag maxdepth=1 maxtree= 67,54,99 | 88.9% | 10/90 | 0/90 | 90.0% | 9/90 | 0/90 | 90.0% | 9/90 | 0/90 |
| Alpha complex | BF with $L=50$ | AdaBag maxdepth=1 maxtree= 27,11,42 | 93.3% | 6/90 | 0/90 | 90.0% | 9/90 | 0/90 | 90.0% | 9/90 | 0/90 |

Table 8: Results using repeated NN with different simplicial complexes and BF of different bin numbers.

| Steps 1&2 | Step 3 | Step 4 | Network Architecture | Accuracy by Class | | | | Error Rates | |
|---------------|-----------------------|--------------|----------------------|--------------------------|--------------|-------------|---------|--------------|---------------|
| | | | | Mixed α - β | All α | All β | Overall | Type-I Error | Type-II Error |
| Rips complex | BF with $L=20, N=40$ | Repeated Net | 86-16-3 | 76.7% | 93.3% | 83.3% | 84.4%* | 14/90 | 0/90 |
| Rips complex | BF with $L=20, N=80$ | Repeated Net | 155-16-3 | 70.0% | 96.7% | 90.0% | 85.6% | 13/90 | 0/90 |
| Rips complex | BF with $L=20, N=200$ | Repeated Net | 325-16-3 | 73.3% | 90.0% | 93.3% | 85.6% | 13/90 | 0/90 |
| Alpha complex | BF with $L=50, N=100$ | Repeated Net | 113-16-3 | 60.0% | 100% | 93.3% | 84.4% | 14/90 | 0/90 |
| Alpha complex | BF with $L=50, N=200$ | Repeated Net | 207-16-3 | 70.0% | 93.3% | 93.3% | 85.6% | 13/90 | 0/90 |
| Alpha complex | BF with $L=50, N=500$ | Repeated Net | 513-16-3 | 80.0% | 93.3% | 93.3% | 88.9% | 10/90 | 0/90 |

Table 9: Results using deep NN with different simplicial complexes and BF of different bin numbers.

| Steps 1&2 | Step 3 | Step 4 | Network Architecture | No dropout | | | With dropout | | |
|---------------|-----------------------|----------|----------------------|------------|--------------|---------------|--------------|--------------|---------------|
| | | | | Overall | Type-I Error | Type-II Error | Overall | Type-I Error | Type-II Error |
| Rips complex | BF with $L=20, N=40$ | Deep Net | 86-128-128-256-3 | 90.0% | 9/90 | 0/90 | 91.1%* | 8/90 | 0/90 |
| Rips complex | BF with $L=20, N=80$ | Deep Net | 155-256-256-512-3 | 90.0% | 9/90 | 0/90 | 90.0% | 9/90 | 0/90 |
| Rips complex | BF with $L=20, N=200$ | Deep Net | 325-512-512-1024-3 | 81.1% | 17/90 | 0/90 | 85.6% | 13/90 | 0/90 |
| Alpha complex | BF with $L=50, N=100$ | Deep Net | 113-128-128-256-3 | 87.8% | 11/90 | 0/90 | 88.9% | 10/90 | 0/90 |
| Alpha complex | BF with $L=50, N=200$ | Deep Net | 207-256-256-512-3 | 88.9% | 10/90 | 0/90 | 91.1% | 8/90 | 0/90 |
| Alpha complex | BF with $L=50, N=500$ | Deep Net | 513-512-512-1024-3 | 86.7% | 12/90 | 0/90 | 82.2% | 16/90 | 0/90 |

References

- Dionysus: the persistent homology software. Software available at <http://www.mrzv.org/software/dionysus>.
- H. Adams, T. Emerson, M. Kirby, R. Neville, C. Peterson, P. Shipman, S. Chepushtanova, E. Hanson, F. Motta, and L. Ziegelmeier. Persistence images: A stable vector representation of persistent homology. *The Journal of Machine Learning Research*, 18(1):218–252, 2017.
- A. Adcock, E. Carlsson, and G. Carlsson. The ring of algebraic functions on persistence bar codes. *Homology, Homotopy and Applications*, 18(1):381–402, 2016.
- M. Ahmed, B. T. Fasy, and C. Wenk. Local persistent homology based distance between maps. In *Proceedings of the 22nd ACM SIGSPATIAL International Conference on Advances in Geographic Information Systems*, pages 43–52. ACM, 2014.
- Esteban Alfaro, Matías Gámez, and Noelia García. adabag: An r package for classification with boosting and bagging. *Journal of Statistical Software*, 54(2), 2013. doi: 10.18637/jss.v054.i02.
- R. Anirudh, J. J. Thiagarajan, I. Kim, and W. Polonik. Autism spectrum disorder classification using graph kernels on multidimensional time series. *arXiv preprint arXiv:1611.09897*, 2016a.
- R. Anirudh, V. Venkataraman, K. N. Ramamurthy, and P. Turaga. A Riemannian framework for statistical analysis of topological persistence diagrams. In *Proceedings of the IEEE Conference on Computer Vision and Pattern Recognition Workshops*, pages 68–76, 2016b.
- W. Bae, J. J. Yoo, and J. C. Ye. Beyond deep residual learning for image restoration: Persistent homology-guided manifold simplification. In *CVPR Workshops*, pages 1141–1149, 2017.
- U. Bauer. Ripser: a lean C++ code for the computation of Vietoris-Rips persistence barcodes. *Software available at <https://github.com/Ripser/ripser>*, 2017.
- U. Bauer, M. Kerber, and J. Reininghaus. Distributed computation of persistent homology. *Proceedings of the Sixteenth Workshop on Algorithm Engineering and Experiments (ALENEX)*, 2014a.
- U. Bauer, M. Kerber, and J. Reininghaus. Distributed computation of persistent homology. In *2014 proceedings of the sixteenth workshop on algorithm engineering and experiments (ALENEX)*, pages 31–38. SIAM, 2014b.
- U. Bauer, M. Kerber, J. Reininghaus, and H. Wagner. PHAT—persistent homology algorithms toolbox. In *International Congress on Mathematical Software*, pages 137–143. Springer, 2014c.
- P. Bendich, D. Cohen-Steiner, H. Edelsbrunner, J. Harer, and D. Morozov. Inferring local homology from sampled stratified spaces. In *Foundations of Computer Science, 2007. FOCS’07. 48th Annual IEEE Symposium on*, pages 536–546. IEEE, 2007.
- P. Bendich, H. Edelsbrunner, and M. Kerber. Computing robustness and persistence for images. *IEEE Transactions on Visualization and Computer Graphics*, 16:1251–1260, 2010.
- P. Bendich, B. Wang, and S. Mukherjee. Local homology transfer and stratification learning. In *Proceedings of the twenty-third annual ACM-SIAM symposium on Discrete Algorithms*, pages 1355–1370. SIAM, 2012.
- P. Bendich, E. Gasparovic, J. Harer, R. Izmailov, and L. Ness. Multi-scale local shape analysis and feature selection in machine learning applications. In *Neural Networks (IJCNN), 2015 International Joint Conference on*, pages 1–8. IEEE, 2015.

- J. Binchi, E. Merelli, M. Rucco, G. Petri, and F. Vaccarino. jholes: A tool for understanding biological complex networks via clique weight rank persistent homology. *Electronic Notes in Theoretical Computer Science*, 306:5–18, 2014.
- T. Bonis, M. Ovsjanikov, S. Oudot, and F. Chazal. Persistence-based pooling for shape pose recognition. In *International Workshop on Computational Topology in Image Context*, pages 19–29. Springer, 2016.
- L. Breiman, J. Friedman, C. J. Stone, and R. A. Olshen. *Classification and Regression Trees*. Wadsworth Statistics/Probability. Chapman and Hall/CRC, 1984. ISBN 9780412048418.
- Leo Breiman. Random forests. *Machine Learning*, 45(1):5–32, 2001. ISSN 1573-0565. doi: 10.1023/A:1010933404324. URL <http://dx.doi.org/10.1023/A:1010933404324>.
- P. Bubenik. Statistical topological data analysis using persistence landscapes. *The Journal of Machine Learning Research*, 16(1):77–102, 2015.
- P. Bubenik and P. Dłotko. A persistence landscapes toolbox for topological statistics. *Journal of Symbolic Computation*, 78:91–114, 2017.
- P. Bubenik and P. T. Kim. A statistical approach to persistent homology. *Homology, Homotopy and Applications*, 19:337–362, 2007.
- Tony Cai and Weidong Liu. A direct estimation approach to sparse linear discriminant analysis. *Journal of the American Statistical Association*, 106(496):1566–1577, dec 2011. doi: 10.1198/jasa.2011.tm11199.
- Z. X. Cang and G. W. Wei. Analysis and prediction of protein folding energy changes upon mutation by element specific persistent homology. *Bioinformatics*, 33(22):3549–3557, 2017a.
- Z. X. Cang and G. W. Wei. Integration of element specific persistent homology and machine learning for protein-ligand binding affinity prediction. *International journal for numerical methods in biomedical engineering*, page 10.1002/cnm.2914, 2017b.
- Z. X. Cang and G. W. Wei. TopologyNet: Topology based deep convolutional and multi-task neural networks for biomolecular property predictions. *PLOS Computational Biology*, 13(7):e1005690, 2017c.
- Z. X. Cang, L. Mu, K. D. Wu, K. Opron, K. L. Xia, and G.W. Wei. A topological approach to protein classification. *Molecular based Mathematical Biologys*, 3:140–162, 2015.
- Z. X. Cang, L. Mu, and G. W. Wei. Representability of algebraic topology for biomolecules in machine learning based scoring and virtual screening. *PLoS computational biology*, 14(1):e1005929, 2018.
- G. Carlsson. Topology and data. *Am. Math. Soc*, 46(2):255–308, 2009.
- G. Carlsson and A. Zomorodian. The theory of multidimensional persistence. *Discrete Computational Geometry*, 42(1):71–93, 2009.
- G. Carlsson, T. Ishkhanov, V. Silva, and A. Zomorodian. On the local behavior of spaces of natural images. *International Journal of Computer Vision*, 76(1):1–12, 2008.
- G. Carlsson, G. Singh, and A. Zomorodian. Computing multidimensional persistence. In *Algorithms and computation*, pages 730–739. Springer, 2009.

- M. Carriere and U. Bauer. On the metric distortion of embedding persistence diagrams into reproducing kernel hilbert spaces. *arXiv preprint arXiv:1806.06924*, 2018.
- M. Carriere, M. Cuturi, and S. Oudot. Sliced wasserstein kernel for persistence diagrams. *arXiv preprint arXiv:1706.03358*, 2017.
- A. Cerri and C. Landi. The persistence space in multidimensional persistent homology. In *Discrete Geometry for Computer Imagery*, pages 180–191. Springer, 2013.
- Chih-Chung Chang and Chih-Jen Lin. LIBSVM: A library for support vector machines. *ACM Transactions on Intelligent Systems and Technology*, 2:27:1–27:27, 2011. Software available at <http://www.csie.ntu.edu.tw/~cjlin/libsvm>.
- F. Chazal, D. Cohen-Steiner, and Q. Mérigot. Geometric inference for probability measures. *Foundations of Computational Mathematics*, 11(6):733–751, 2011.
- F. Chazal, B. Fasy, F. Lecci, B. Michel, A. Rinaldo, A. Rinaldo, and L. Wasserman. Robust topological inference: Distance to a measure and kernel distance. *The Journal of Machine Learning Research*, 18(1):5845–5884, 2017.
- Y. Chen, E. K. Garcia, M. R. Gupta, A. Rahimi, and L. Cazzanti. Similarity-based classification: Concepts and algorithms. *Journal of Machine Learning Research*, 10:747–776, March 2009.
- I. Chevyrev, V. Nanda, and H. Oberhauser. Persistence paths and signature features in topological data analysis. *arXiv preprint arXiv:1806.00381*, 2018.
- H. Chintakunta, T. Gentimis, R. Gonzalez-Diaz, M. J. Jimenez, and H. Krim. An entropy-based persistence barcode. *Pattern Recognition*, 48(2):391–401, 2015.
- Mei Choi Chiu, Chi Seng Pun, and Hoi Ying Wong. Big data challenges of high-dimensional continuous-time mean-variance portfolio selection and a remedy. *Risk Analysis*, 37(8):1532–1549, mar 2017. doi: 10.1111/risa.12801.
- D. Cohen-Steiner, H. Edelsbrunner, and D. Morozov. Vines and vineyards by updating persistence in linear time. In *Proceedings of the twenty-second annual symposium on Computational geometry*, pages 119–126. ACM, 2006.
- C. Cortes and V. Vapnik. Support-vector networks. *Machine learning*, 20(3):273–297, 1995. doi: <https://doi.org/10.1023/A:1022627411411>.
- T. K. Dey and S. Mandal. Protein classification with improved topological data analysis. In *LIPICs-Leibniz International Proceedings in Informatics*, volume 113. Schloss Dagstuhl-Leibniz-Zentrum fuer Informatik, 2018.
- T. K. Dey and Y. S. Wang. Reeb graphs: Approximation and persistence. *Discrete and Computational Geometry*, 49(1):46–73, 2013. ISSN 0179-5376. doi: 10.1007/s00454-012-9463-z. URL <http://dx.doi.org/10.1007/s00454-012-9463-z>.
- T. K. Dey, K. Y. Li, J. Sun, and C. S. David. Computing geometry aware handle and tunnel loops in 3d models. *ACM Trans. Graph.*, 27, 2008.
- B. Di Fabio and C. Landi. A Mayer-Vietoris formula for persistent homology with an application to shape recognition in the presence of occlusions. *Foundations of Computational Mathematics*, 11: 499–527, 2011.
- H. Edelsbrunner and J. Harer. *Computational topology: an introduction*. American Mathematical Soc., 2010.

- H. Edelsbrunner and E. P. Mücke. Three-dimensional alpha shapes. *Physical Review Letters*, 13: 43–72, 1994.
- H. Edelsbrunner, D. Letscher, and A. Zomorodian. Topological persistence and simplification. *Discrete Comput. Geom.*, 28:511–533, 2002.
- Herbert Edelsbrunner. Weighted alpha shapes. Technical report, Champaign, IL, USA, 1992.
- R.-E. Fan, K.-W. Chang, C.-J. Hsieh, X.-R. Wang, , and C.-J. Lin. Liblinear: A library for large linear classification. *Journal of Machine Learning Research*, 9:1871–1874, 2008.
- B. T. Fasy and B. Wang. Exploring persistent local homology in topological data analysis. In *Acoustics, Speech and Signal Processing (ICASSP), 2016 IEEE International Conference on*, pages 6430–6434. IEEE, 2016.
- B. T. Fasy, J. Kim, F. Lecci, and C. Maria. Introduction to the r package tda. *arXiv preprint arXiv:1411.1830*, 2014.
- Naomi K Fox, Steven E Brenner, and John-Marc Chandonia. Scope: Structural classification of proteins-extended, integrating scop and astral data and classification of new structures. *Nucleic Acids Research*, 42(D1):D304–D309, 2014.
- Y. Freund and Schapire. A decision-theoretic generalization of on-line learning and an application to boosting. *Journal of Computer and System Sciences*, 55(1):119–139, aug 1997. doi: 10.1006/jcss.1997.1504.
- J. H. Friedman. Greedy function approximation: A gradient boosting machine. *Annals of statistics*, 29(5):1189–1232, 2001.
- A. Frohmader. Face vectors of flag complexes. *Israel Journal of Mathematics*, 164(1):153–164, 2008.
- P. Frosini and C. Landi. Persistent Betti numbers for a noise tolerant shape-based approach to image retrieval. *Pattern Recognition Letters*, 34(8):863–872, 2013.
- M. Gameiro, Y. Hiraoka, S. Izumi, M. Kramar, K. Mischaikow, and V. Nanda. Topological measurement of protein compressibility via persistence diagrams. *preprint*, 2013.
- R. Ghrist. Barcodes: The persistent topology of data. *Bull. Amer. Math. Soc.*, 45:61–75, 2008a.
- R. Ghrist. Barcodes: the persistent topology of data. *Bulletin of the American Mathematical Society*, 45(1):61–75, 2008b.
- N. Giansiracusa, R. Giansiracusa, and C. Moon. Persistent homology machine learning for fingerprint classification. *arXiv preprint arXiv:1711.09158*, 2017.
- C. Giusti, E. Pastalkova, C. Curto, and V. Itskov. Clique topology reveals intrinsic geometric structure in neural correlations. *Proceedings of the National Academy of Sciences*, 112(44):13455–13460, 2015.
- W. Guo, K. Manohar, S. L. Brunton, and A. G. Banerjee. Sparse-tda: Sparse realization of topological data analysis for multi-way classification. *IEEE Transactions on Knowledge and Data Engineering*, 30(7):1403–1408, 2018.
- M. Z. Hadimaja and C. S. Pun. A self-calibrated regularized direct estimation for graphical selection and discriminant analysis. *Working paper*, 2018.
- Y. S. Han, J. Yoo, and J. C. Ye. Deep residual learning for compressed sensing ct reconstruction via persistent homology analysis. *arXiv preprint arXiv:1611.06391*, 2016.

- Trevor Hastie, Robert Tibshirani, and Jerome Friedman. The elements of statistical learning: Data mining, inference, and prediction. In *The Elements of Statistical Learning: Data Mining, Inference, and Prediction*, Second Edition. Springer, 2009.
- Y. Hiraoka, T. Nakamura, A. Hirata, E. G. Escolar, K. Matsue, and Y. Nishiura. Hierarchical structures of amorphous solids characterized by persistent homology. *Proceedings of the National Academy of Sciences*, 113(26):7035–7040, 2016.
- C. Hofer, R. Kwitt, M. Niethammer, and A. Uhl. Deep learning with topological signatures. In *Advances in Neural Information Processing Systems*, pages 1634–1644, 2017.
- D. Horak, S. Maletic, and M. Rajkovic. Persistent homology of complex networks. *Journal of Statistical Mechanics: Theory and Experiment*, 2009(03):P03034, 2009. URL <http://stacks.iop.org/1742-5468/2009/i=03/a=P03034>.
- Lajos Horváth and Piotr Kokoszka. *Inference for Functional Data with Applications*. Springer New York, 2012. doi: 10.1007/978-1-4614-3655-3.
- T. Kaczynski, K. Mischaikow, and M. Mrozek. *Computational homology*. Springer-Verlag, 2004.
- S. Kališnik. Tropical coordinates on the space of persistence barcodes. *Foundations of Computational Mathematics*, pages 1–29, 2018.
- P. M. Kasson, A. Zomorodian, S. Park, N. Singhal, L. J. Guibas, and V. S. Pande. Persistent voids a new structural metric for membrane fusion. *Bioinformatics*, 23:1753–1759, 2007.
- G. Kusano, Y. Hiraoka, and K. Fukumizu. Persistence weighted gaussian kernel for topological data analysis. In *International Conference on Machine Learning*, pages 2004–2013, 2016.
- R. Kwitt, S. Huber, M. Niethammer, W. Lin, and U. Bauer. Statistical topological data analysis—a kernel perspective. In *Advances in neural information processing systems*, pages 3070–3078, 2015.
- T. Le and M. Yamada. Riemannian manifold kernel for persistence diagrams. *arXiv preprint arXiv:1802.03569*, 2018.
- H. Lee, H. Kang, M. K. Chung, B. Kim, and D. S. Lee. Persistent brain network homology from the perspective of dendrogram. *Medical Imaging, IEEE Transactions on*, 31(12):2267–2277, Dec 2012. ISSN 0278-0062. doi: 10.1109/TMI.2012.2219590.
- C. Li, M. Ovsjanikov, and F. Chazal. Persistence-based structural recognition. In *Proceedings of the IEEE Conference on Computer Vision and Pattern Recognition*, pages 1995–2002, 2014.
- Henry W. Lin, Max Tegmark, and David Rolnick. Why does deep and cheap learning work so well? *Journal of Statistical Physics*, 168(6):1223–1247, jul 2017. doi: 10.1007/s10955-017-1836-5.
- X. Liu, Z. Xie, and D. Y. Yi. A fast algorithm for constructing topological structure in large data. *Homology, Homotopy and Applications*, 14:221–238, 2012.
- N. Makarenko, M. Kalimoldayev, I. Pak, and A. Yessenaliyeva. Texture recognition by the methods of topological data analysis. *Open Engineering*, 6(1), 2016.
- A. Marchese and V. Maroulas. Signal classification with a point process distance on the space of persistence diagrams. *Advances in Data Analysis and Classification*, pages 1–26, 2017.
- C. Maria. Filtered complexes. In *GUDHI User and Reference Manual*. GUDHI Editorial Board, 2015. URL http://gudhi.gforge.inria.fr/doc/latest/group__simplex__tree.html.

- E. Merelli, M. Rucco, P. Sloot, and L. Tesei. Topological characterization of complex systems: Using persistent entropy. *Entropy*, 17(10):6872–6892, 2015.
- Y. Mileyko, S. Mukherjee, and J. Harer. Probability measures on the space of persistence diagrams. *Inverse Problems*, 27(12):124007, 2011.
- K. Mischaikow and V. Nanda. Morse theory for filtrations and efficient computation of persistent homology. *Discrete and Computational Geometry*, 50(2):330–353, 2013. ISSN 0179-5376. doi: 10.1007/s00454-013-9529-6. URL <http://dx.doi.org/10.1007/s00454-013-9529-6>.
- K. Mischaikow, M Mrozek, J. Reiss, and A. Szymczak. Construction of symbolic dynamics from experimental time series. *Physical Review Letters*, 82:1144–1147, 1999.
- J. R. Munkres. *Elements of algebraic topology*. CRC Press, 2018.
- A. G. Murzin, S. E. Brenner, T. Hubbard, and C. Chothia. SCOP: a structural classification of proteins database for the investigation of sequences and structures. *Journal of molecular biology*, 247(4):536–540, 1995.
- Vidit Nanda. Perseus: the persistent homology software. Software available at <http://www.sas.upenn.edu/~vnanda/perseus>.
- D. D. Nguyen, T. Xiao, M. L. Wang, and G. W. Wei. Rigidity strengthening: A mechanism for protein–ligand binding. *Journal of chemical information and modeling*, 57(7):1715–1721, 2017.
- D. D. Nguyen, Z. X. Cang, K. D. Wu, M. L. Wang, Y. Cao, and G. W. Wei. Mathematical deep learning for pose and binding affinity prediction and ranking in D3R Grand Challenges. *arXiv preprint arXiv:1804.10647*, 2018.
- P. Niyogi, S. Smale, and S. Weinberger. A topological view of unsupervised learning from noisy data. *SIAM Journal on Computing*, 40:646–663, 2011a.
- P. Niyogi, S. Smale, and S. Weinberger. A topological view of unsupervised learning from noisy data. *SIAM Journal on Computing*, 40(3):646–663, 2011b.
- I. Obayashi, Y. Hiraoka, and M. Kimura. Persistence diagrams with linear machine learning models. *Journal of Applied and Computational Topology*, 1(3-4):421–449, 2018.
- D. Pachauri, C. Hinrichs, M. K. Chung, S. C. Johnson, and V. Singh. Topology-based kernels with application to inference problems in alzheimer’s disease. *IEEE transactions on medical imaging*, 30(10):1760–1770, 2011a.
- D. Pachauri, C. Hinrichs, M.K. Chung, S.C. Johnson, and V. Singh. Topology-based kernels with application to inference problems in alzheimer’s disease. *Medical Imaging, IEEE Transactions on*, 30(10):1760–1770, Oct 2011b. ISSN 0278-0062. doi: 10.1109/TMI.2011.2147327.
- T. Padellini and P. Brutti. Supervised learning with indefinite topological kernels. *arXiv preprint arXiv:1709.07100*, 2017.
- Chi Seng Pun. A sparse learning approach to relative-volatility-managed portfolio selection. *Available at SSRN.com/abstract=3179569*, 2018.
- Chi Seng Pun and Hoi Ying Wong. Resolution of degeneracy in merton’s portfolio problem. *SIAM Journal on Financial Mathematics*, 7(1):786–811, jan 2016. doi: 10.1137/16m1065021.
- Chi Seng Pun and Hoi Ying Wong. A linear programming model for selection of sparse high-dimensional multiperiod portfolios. *European Journal of Operational Research*, aug 2018. doi: 10.1016/j.ejor.2018.08.025.

- T. Qaiser, Y. W. Tsang, D. Taniyama, N. Sakamoto, K. Nakane, D. Epstein, and N. Rajpoot. Fast and accurate tumor segmentation of histology images using persistent homology and deep convolutional features. *arXiv preprint arXiv:1805.03699*, 2018.
- J. O. Ramsay and B. W. Silverman. *Functional Data Analysis*. Springer New York, 1997. doi: 10.1007/978-1-4757-7107-7.
- J. Reininghaus, S. Huber, U. Bauer, and R. Kwitt. A stable multi-scale kernel for topological machine learning. In *Proceedings of the IEEE conference on computer vision and pattern recognition*, pages 4741–4748, 2015.
- Shiquan Ren, Chengyuan Wu, and Jie Wu. Weighted persistent homology. *arXiv preprint arXiv:1708.06722*, 2017.
- B. Rieck, H. Mara, and H. Leitte. Multivariate data analysis using persistence-based filtering and topological signatures. *IEEE Transactions on Visualization and Computer Graphics*, 18:2382–2391, 2012.
- V. Robins and K. Turner. Principal component analysis of persistent homology rank functions with case studies of spatial point patterns, sphere packing and colloids. *Physica D: Nonlinear Phenomena*, 334:99–117, 2016.
- M. Rucco, F. Castiglione, E. Merelli, and M. Pettini. Characterisation of the idiotypic immune network through persistent entropy. In *Proceedings of ECCS 2014*, pages 117–128. Springer, 2016.
- M. Saadatfar, H. Takeuchi, V. Robins, N. Francois, and Y. Hiraoka. Pore configuration landscape of granular crystallization. *Nature communications*, 8:15082, 2017.
- L. M. Seversky, S. Davis, and M. Berger. On time-series topological data analysis: New data and opportunities. In *Proceedings of the IEEE Conference on Computer Vision and Pattern Recognition Workshops*, pages 59–67, 2016.
- V. D. Silva and R. Ghrist. Blind swarms for coverage in 2-d. In *In Proceedings of Robotics: Science and Systems*, page 01, 2005.
- G. Singh, F. Memoli, T. Ishkhanov, G. Sapiro, G. Carlsson, and D. L. Ringach. Topological analysis of population activity in visual cortex. *Journal of Vision*, 8(8), 2008. doi: 10.1167/8.8.11. URL <http://www.journalofvision.org/content/8/8/11.abstract>.
- Nitish Srivastava, Geoffrey Hinton, Alex Krizhevsky, Ilya Sutskever, and Ruslan Salakhutdinov. Dropout: A simple way to prevent neural networks from overfitting. *Journal of Machine Learning Research*, 15:1929–1958, 2014.
- Andrew Tausz, Mikael Vejdemo-Johansson, and Henry Adams. Javaplex: A research software package for persistent (co)homology. Software available at <http://code.google.com/p/javaplex>, 2011.
- K. Turner, Y. Mileyko, S. Mukherjee, and J. Harer. Fréchet means for distributions of persistence diagrams. *Discrete & Computational Geometry*, 52(1):44–70, 2014.
- Y. Umeda. Time series classification via topological data analysis. *Information and Media Technologies*, 12:228–239, 2017.
- B. Wang and G. W. Wei. Object-oriented persistent homology. *Journal of Computational Physics*, 305:276–299, 2016.

- B. Wang, B. Summa, V. Pascucci, and M. Vejdemo-Johansson. Branching and circular features in high dimensional data. *IEEE Transactions on Visualization and Computer Graphics*, 17:1902–1911, 2011.
- Y. Wang, H. Ombao, M. K. Chung, et al. Persistence landscape of functional signal and its application to epileptic electroencephalogram data. *ENAR Distinguished Student Paper Award*, 2014.
- Chengyuan Wu, Shiquan Ren, Jie Wu, and Kelin Xia. Weighted (co) homology and weighted laplacian. *arXiv preprint arXiv:1804.06990*, 2018.
- K. D. Wu and G. W. Wei. Quantitative toxicity prediction using topology based multi-task deep neural networks. *Journal of chemical information and modeling*, page 10.1021/acs.jcim.7b00558, 2018.
- K. L. Xia. A quantitative structure comparison with persistent similarity. *arXiv preprint arXiv:1707.03572*, 2017.
- K. L. Xia. Persistent homology analysis of ion aggregations and hydrogen-bonding networks. *Physical Chemistry Chemical Physics*, 20(19):13448–13460, 2018.
- K. L. Xia and G. W. Wei. Persistent homology analysis of protein structure, flexibility and folding. *International Journal for Numerical Methods in Biomedical Engineerings*, 30:814–844, 2014.
- K. L. Xia and G. W. Wei. Persistent topology for cryo-EM data analysis. *International Journal for Numerical Methods in Biomedical Engineering*, 31:e02719, 2015a.
- K. L. Xia and G. W. Wei. Multidimensional persistence in biomolecular data. *Journal Computational Chemistry*, 36:1502–1520, 2015b.
- K. L. Xia, X. Feng, Y. Y. Tong, and G. W. Wei. Persistent homology for the quantitative prediction of fullerene stability. *Journal of Computational Chemistry*, 36:408–422, 2015a.
- K. L. Xia, Z. X. Zhao, and G. W. Wei. Multiresolution topological simplification. *Journal Computational Biology*, 22:1–5, 2015b.
- K. L. Xia, Z. M. Li, and L. Mu. Multiscale persistent functions for biomolecular structure characterization. *Bulletin of mathematical biology*, 80(1):1–31, 2018.
- Y. Yao, J. Sun, X. H. Huang, G. R. Bowman, G. Singh, M. Lesnick, L. J. Guibas, V. S. Pande, and G. Carlsson. Topological methods for exploring low-density states in biomolecular folding pathways. *The Journal of Chemical Physics*, 130:144115, 2009.
- M. Zeppelzauer, B. Zieliński, M. Juda, and M. Seidl. A study on topological descriptors for the analysis of 3d surface texture. *Computer Vision and Image Understanding*, 167:74–88, 2018.
- Z. F. Zhang, Y. Song, H. C. Cui, J. Wu, F. Schwartz, and H. R. Qi. Early mastitis diagnosis through topological analysis of biosignals from low-voltage alternate current electrokinetics. In *Engineering in Medicine and Biology Society (EMBC), 2015 37th Annual International Conference of the IEEE*, pages 542–545. IEEE, 2015.
- Z. Zhou, Y. Z. Huang, L. Wang, and T. N. Tan. Exploring generalized shape analysis by topological representations. *Pattern Recognition Letters*, 87:177–185, 2017.
- X. J. Zhu. Persistent homology: An introduction and a new text representation for natural language processing. In *IJCAI*, pages 1953–1959, 2013.

- B. Zielinski, M. Juda, and M. Zeppelzauer. Persistence codebooks for topological data analysis. *arXiv preprint [arXiv:1802.04852](https://arxiv.org/abs/1802.04852)*, 2018.
- A. Zomorodian. The tidy set: a minimal simplicial set for computing homology of clique complexes. In *Proceedings of the twenty-sixth annual symposium on Computational geometry*, pages 257–266. ACM, 2010.
- A. Zomorodian and G. Carlsson. Computing persistent homology. *Discrete Comput. Geom.*, 33: 249–274, 2005.
- A. Zomorodian and G. Carlsson. Localized homology. *Computational Geometry - Theory and Applications*, 41(3):126–148, 2008.
- A. J. Zomorodian. *Topology for computing*, volume 16. Cambridge university press, 2005.